A new boronate ester-based crosslinking strategy allows the design of nonswelling and long-term stable dynamic covalent hydrogels

N. Lagneau, L. Terriac, P. Tournier, J-J. Helesbeux, Guillaume Viault, D. Séraphin, B. Halgand, F. Loll, Catherine Garnier, C. Jonchère, et al.

A New Boronate Ester-Based Crosslinking Strategy Allows the Design of Nonswelling and Long-Term Stable Dynamic Covalent Hydrogels

N. Lagneau, L. Terriac, P. Tournier, J J. Helesbeux, G. Viault, D. Séraphin, B. Halgand, F. Loll, Catherine Garnier, C. Jonchère, et al.

A New Boronate Ester-Based Crosslinking Strategy Allows the Design of Nonswelling and Long-Term Stable Dynamic Covalent Hydrogels

N. Lagneau,[1] L. Terriac,[1] P. Tournier,[1] J-J. Helesbeux,[2] G. Viault,[2] D. Séraphin,[2] B. Halgand,[1] F. Loll,[1] C. Garnier,[3] C. Jonchère,[3] M. Rivière,[4] A. Tessier,[4] J. Lebreton,[4] Y. Maugars,[1] J. Guicheux,[1] C. Le Visage,[1] V. Delplace.[1,#]

[1]Nantes Université, Oniris, CHU Nantes, INSERM, Regenerative Medicine and Skeleton, RMeS, UMR 1229, F-44000 Nantes, FRANCE

[2]Substances d'Origine Naturelle et Analogues Structuraux, SFR4207 QUASAV, Université d'Angers, Angers, France.

[3]INRAE, UR1268 Biopolymères Interactions Assemblages, F-44300 Nantes, France

[4]Nantes Université, CNRS, CEISAM, UMR 6230, F-44000 Nantes, FRANCE

[#]Corresponding author :
Faculté d'Odontologie, Université de Nantes
1, place Alexis Ricordeau, 44000 Nantes, France
E-mail address: vianney.delplace@univ-nantes.fr (V. Delplace)

Abstract

Dynamic hydrogels are viscoelastic materials that can be designed to be self-healing, malleable, and injectable, making them particularly interesting for a variety of biomedical applications. To design dynamic hydrogels, dynamic covalent crosslinking reactions are attracting increasing attention. However, dynamic covalent hydrogels tend to swell, and often lack stability. Boronate ester-based hydrogels, which result from the dynamic covalent reaction between a phenylboronic acid (PBA) derivative and a diol, are based on stable precursors, and can therefore address these limitations. Yet, boronate ester formation hardly occurs at physiological pH. To produce dynamic covalent hydrogels at physiological pH, we performed a molecular screening of PBA derivatives in association with a variety of diols, using hyaluronic acid as a polymer of interest. The combination of Wulff-type PBA (wPBA) and glucamine stood out as a unique couple to obtain the desired hydrogels. We showed that optimized wPBA/glucamine hydrogels are minimally- to non-swelling, stable long term (over months), tunable in terms of mechanical properties, and cytocompatible. We further characterized their viscoelastic and self-healing properties, highlighting their potential for biomedical applications.

Keywords: hydrogel, hyaluronic acid, boronate ester, viscoelasticity, self-healing

Introduction

Hydrogels are widely used as scaffolds for a variety of biomedical applications, including drug/cell delivery, 3D cell culture and tissue engineering. While many hydrogels are based on covalent crosslinking (e.g., radical polymerization, thiol-ene chemistry), covalent hydrogels are inherently brittle and not injectable.[1] Their elastic properties also do not fully reproduce the viscoelastic properties of natural tissues,[2] limiting their use as synthetic extracellular matrices. In this context, dynamic hydrogels are receiving growing attention for their viscoelastic properties, which make these hydrogels malleable and injectable,[3] and allow them to better mimic the mechanical properties of living tissues.[2]

Dynamic hydrogels can be obtained using non-covalent interactions or dynamic covalent reactions.[1,3–5] Hydrogels based on non-covalent interactions, such as hydrogen bonding or ionic bonding, commonly use polymers with natural crosslinking properties (e.g., alginate with calcium ions), and are therefore inherently limited in terms of polymer composition. Non-covalent hydrogels based on supramolecular interactions require the synthesis of complex and expensive precursors,[6] making them hardly accessible. In contrast, dynamic covalent hydrogels are usually based on well-established dynamic covalent reactions (e.g., Schiff base formation, disulfide formation, Diels-Alder reaction), and are obtained after the straightforward grafting of small molecules on a chosen polymer. This allows for the design of relatively affordable dynamic hydrogels, with tunable composition and mechanical properties.[7] However, dynamic covalent reactions often rely on the use of precursors that have a limited stability at physiological pH, such as thiol, carbonyl or maleimide groups.[8–10] Based on stable precursors, boronate ester formation is a promising alternative for the design of dynamic covalent hydrogels.[11,12]

Boronate ester formation results from the reversible condensation of a boronic acid derivative (typically, a phenylboronic acid [PBA]) with a diol (Figure 1a). One main drawback of this reaction is that it is commonly favored at basic pH, with a chemical equilibrium shifted toward the dissociated molecules at physiological pH. As a consequence, boronate ester-based hydrogels hardly form under physiological conditions.[13,14] Inspired by early works on PBA-based sugar purification techniques,[15,16] new classes of PBAs with decreased pKa values and increased reactivity, including benzoxaboroles (BX) and Wulff-type PBAs (wPBA), have recently been developed to promote PBA/diol crosslinking at physiological pH. The reported PBA/diol couples with effective gelation under physiological conditions include: BX with fructose or glucono-δ-lactone,[17] BX with nopoldiol,[18] BX with nitrodopamine,[19]

FluoroPBA with glucono-δ-lactone,[20] and wPBA with glucono-δ-lactone.[21] These hydrogels presented several limitations, such as a complex and multi-step synthesis,[22] the use of precursors with limited solubility or stability,[19,20] a narrow range of mechanical properties,[17] important swelling,[18,23] or a stability limited to days.[12,21,24–26] Thus, the design of boronate ester-based hydrogels that are easy to synthesize, minimally- to non-swelling, stable long term (over weeks), tunable in terms of mechanical properties, and cytocompatible, remains a challenge. This challenge is particularly true for hydrogels composed of natural polymers, such as hyaluronic acid (HA), as most of the reported systems were based on synthetic polymers.

In this study, we investigated a large variety of PBA/diol couples for the synthesis of boronate ester-based HA hydrogels under physiological conditions. Among the 24 PBA/diol couples tested, the combination of wPBA and glucamine stood out for its unique ability to form hydrogels at physiological pH. We then optimized wPBA/glucamine hydrogel formulations to produce two dynamic covalent hydrogels with minimal swelling and long-term stability in culture medium (over at least 2 months), exhibiting distinct elastic properties (G' of ≈ 100 Pa vs ≈ 1000 Pa, at 1 Hz). Using dynamic shear rheology, we confirmed that these new dynamic covalent hydrogels have frequency-dependent shear moduli, as well as stress relaxation and self-healing properties. Finally, using a L929 murine fibroblasts and human adipose tissue-derived stromal cells (hASCs), we demonstrated the cytocompatibility of the new hydrogels (> 95% viable cells after 7 days of culture). Together, our results highlight the potential of wPBA/glucamine hydrogels for biomedical applications.

Experimental section

Materials

Sodium hyaluronate was purchased from Lifecore Biomedical. Alginate (Protanal LF10/60) was purchased from FMC Corporation. 2-(N-morpholino)ethanesulfonic acid, 4-(4,6-dimethoxy-1,3,5-triazin-2-yl)-4-methylmorpholinium chloride (DMT-MM), 5-Amino-2-(hydroxymethyl)phenylboronic acid cyclic monoester, 2-amino-2-deoxy-D-glucopyranose hydrochloride, 2-amino-2-deoxy-D-galactopyranose hydrochloride and D-glucamine were purchased from TCI Chemicals. 1-amino-1-deoxy-D-galactitol hydrochloride and 1-amino-1-deoxy-D-fructose hydrochloride were purchased from Carbosynth. 6-(aminomethyl)-3-pyridylboronic acid was purchased from Advanced ChemBlocks. Dulbecco's Phosphate Buffered Saline (without Ca & Mg), Dulbecco's Modified Eagle Medium (DMEM), Roswell Park Memorial Institute medium (RPMI), Promocell medium, Penicillin/Streptomycin,

Live/Dead and Picogreen Kit were purchased from ThermoFischer Scientific. L929 cells were purchased from ATCC. Fetal Bovine serum (FBS) was purchased from Dominique Dutscher. Growth medium was purchased from Promocell. Otherwise stated, all other reagents were purchased from Sigma-Aldrich.

Methods

Small molecule synthesis

Synthesis of Wulff-type phenylboronic acid: The detailed synthetic procedure of wPBA is available as supplementary information, with the corresponding NMR spectra (Figure S1 and S2). Briefly, tert-butyl(4-aminobutyl)carbamate (7.30 g, 38.80 mmol), which was synthesized in house, was dissolved in methanol (30 mL). 2-formylphenylboronic acid (5.82 g, 38.80 mmol) was added and allowed to react overnight under stirring at room temperature. Then, sodium borohydride (1.21g, 32.08 mmol) was added at 0 °C, and allowed to react at room temperature until bubbles disappeared. Organic layers were extracted using dichloromethane (DCM), then dried over Na_2SO_4, and concentrated under reduced pressure to obtain 2-(((4-((tert-butoxycarbonyl)amino)butyl)amino)methyl) phenyl)boronic acid (protected wPBA) (yield = 95%). Finally, (2-(((4-aminobutyl)amino) methyl)phenyl)boronic acid (wPBA) was obtained by deprotecting the primary amine of the protected wPBA (2.62 mmol in 5 mL methanol) with hydrogen chloride gas (from sulfuric acid over NaCl) at 0 °C under argon atmosphere. Organic layers were extracted using dichloromethane (DCM), then dried over Na_2SO_4, to obtain wPBA (427 mg, 1.89 mmol; yield = 72%).

Synthesis of iditolamine: Iditolamine was synthesized as previously described,[27] with some modifications. Briefly, to a solution of 1-deoxy-1-nitro-iditol (100 mg, 0.47 mmol) in 10 mL of methanol, Pd/C (10% [w/w]) and trifluoroacetic acid (100 µL) were added. The reaction mixture was stirred at room temperature and H_2 was bubbled through the suspension for 15 min. Then the reaction mixture was heated at 100 °C under microwave irradiations for 1 hour. This sequence was repeated until total consumption of the starting material determined by TLC monitoring (SiO_2, EtOAc/MeOH/NH_3 50/50/1). The catalyst was then filtered over a celite pad. The filtrate was concentrated under vacuum and purified by flash column chromatography using silica gel with a EtOH/H_2O gradient as eluent (100/0 to 10/90) leading to the iditolamine TFA salt (67.6 mg, 0.23 mmol, yield = 49%). NMR data are provided as supplementary information (Figure S3 and S4).

Synthesis of HA-PBAs: The investigated PBAs were 2-aminophenylboronic acid (2PBA), 3-aminophenylboronic acid (3PBA), 4-aminophenylboronic acid (4PBA), 2-aminopyrimidine-

5-boronic acid (PymBA), 6-(aminomethyl)-3-pyridylboronic acid (PydBA) and 5-Amino-2-(hydroxymethyl)phenylboronic acid cyclic monoester (Benzoxaborole, BX). HA-2PBA, HA-3PBA, HA-4PBA, HA-PymBA, HA-PydBA and HA-BX were synthesized, as follows: HA (100 mg, 0.248 mmol of carboxylic acid) was dissolved in MES buffer pH 5.5 (9 mL) under stirring at room temperature. DMT-MM (34 mg, 0.124 mmol; 0.5 eq relative to carboxylic acid) was added and allowed to react for 30 min. Then, a chosen PBA (0.25 eq relative to carboxylic acid) was dissolved in DMSO (1mL) and added dropwise to the polymer solution. The solution was dialyzed against 0.1 M DPBS for 1 day, then against deionized water for 2 days, before filter sterilization, lyophilization, and storage at -20 °C. The degrees of substitution (DS) of HA-wPBA and HA-2PBA were determined by ^{1}H NMR (400 MHz, D_2O) using the 3 protons of the N-acetyl group of HA (2.1 ppm) as a reference to calculate the relative amount of grafted PBAs (4 protons between 7.5-8 ppm). The DS of HA-4PBA and HA-BX were determined by elemental analysis using the following equation : $DS = \frac{N_{HA} - C_{HA} * (\frac{N}{C})^{-1}}{\frac{N}{C} * C_{PBA} - N_{PBA}}$, with N_{HA}, the number of nitrogens of HA ; C_{HA}, the number of carbons of HA ; N_{PBA}, the number of nitrogens of the grafted PBA ; C_{PBA}, the number of carbons of the grafted PBA ; and N/C, the experimental molar ratio of nitrogens and carbons (details on elemental analysis data are provided in Table S3). The synthetic conditions of all HA-PBAs are summarized in Table S1.

Synthesis of HA-wPBA: HA-wPBA was typically synthesized as follows: HA (100 mg, 0.248 mmol of carboxylic acid) was dissolved in MES buffer pH 5.5 (10 mL) under stirring at room temperature. DMT-MM (69 mg, 0.248 mmol; 1 eq relative to carboxylic acid) was added and allowed to react for 30 min. Then, 2-(4-aminobutyl) aminomethylphenylboronic acid (Wulff-type PBA, wPBA) (28 mg, 0.124 mmol; 0.5 eq relative to carboxylic acid) was added to the polymer solution. The solution was dialyzed against 0.1 M DPBS for 1 day, then against deionized water for 2 days, before filter sterilization, lyophilization, and storage at -20 °C. DS was determined by ^{1}H NMR (400 MHz, D_2O) and elemental analysis. A similar procedure was applied for the synthesis of alginate-wPBA. The synthetic conditions of the HA-wPBAs are summarized in Table S1.

Synthesis of HA-diol: The investigated diols were tris(hydroxyméthyl)aminomethane (tris), 3-amino-1,2-propanediol (aminopropanediol), 2-amino-1,3-propanediol (serinol), 2-amino-2-deoxy-D-glucopyranose (glucosamine), 2-amino-2-deoxy-D-galactopyranose (galactosamine), 1-amino-1-deoxy-D-fructose (fructosamine), 1-amino-1-deoxy-D-galactitol

(dulcitolamine), 1-amino-1-deoxy-D-sorbitol (glucamine) and 1-amino-1-deoxy-D-iditol (iditolamine) and 4-(2-aminoethyl)benzene-1,2-diol (dopamine). HA-diol was synthesized, as follows: HA (100 mg, 0.248 mmol of carboxylic acid) was dissolved in MES buffer pH 5.5 (10 mL) under stirring at room temperature. DMT-MM (69 mg, 0.248 mmol; 1 eq relative to carboxylic acid) was added and allowed to react for 30 min. Then, a chosen amino diol (0.5 eq relative to carboxylic acid) was added to the polymer solution. The solution was dialyzed against 0.1 M DPBS for 1 day, then against deionized water for 2 days, before filter sterilization, lyophilization, and storage at -20 °C. DS were determined by unreacted amine dosage (2,4,6-Trinitrobenzenesulfonic acid; TNBS) and elemental analysis. DS by elemental analysis was determined using a similar procedure to that described above (details on elemental analysis data are provided in Table S3). A similar procedure was applied for the synthesis of alginate-glucamine. The synthetic conditions of all HA-diols are summarized in Table S2.

Synthesis of fluorescent HA-glucamine: HA-glucamine (50 mg) was dissolved in MES buffer pH 5.5 (4.5 mL), under stirring at room temperature. 3 mg of DMT-MM (large excess relative to hydrazide) were added and allowed to react for 30 min. Then, CF™ 488A hydrazide (0.5 mg, 0.54 µmol) or CF™ 647 hydrazide (0.5 mg, 0.17 µmol) was dissolved in DMSO (0.5 mL), added to the polymer solution, and allowed to react in the dark for 3 days, under stirring at room temperature. The solution was dialyzed against 0.1 M DPBS with 2% DMSO for 24 h, then 0.1 M DPBS for 8 hours, and deionized water for 48 hours, prior to filter-sterilization, lyophilization and storage at -20 °C.

Hydrogel formation and characterization

Hydrogel formation and screening: Hydrogels were obtained by separately dissolving an HA-PBA and an HA-diol, either in PBS or culture medium (DMEM, RPMI or Promocell), prior to mixing them together in a chosen volume ratio, at room temperature. The initial concentrations and volume ratios of the two components were calculated based on the desired final HA content and PBA:diol molar ratio. The screening of PBA/diol couples was carried out at 1% (w/v) HA content, with a PBA:diol molar ratio of 1:1.

Rheological characterization: Oscillatory shear experiments were performed using a HAAKE™ MARS™ (ThermoFischer Scientific) equipped with a 20-mm titanium upper plate at 37 °C with a solvent trap to prevent evaporation. Pre-hydrogel solutions were prepared as described above, and measurements were performed immediately after the mixing of the two

hydrogel precursors. Frequency sweep experiments were performed at a constant stress of 1 Pa. Time sweep experiments were conducted at a constant stress of 1 Pa and a constant frequency of 1 Hz (within the linear viscoelastic region). Self-healing experiments were performed at a constant frequency of 1 Hz, with alternated stress of 1 Pa and 250 Pa (soft formulation), or 1 Pa and 1200 Pa (stiff formulation). Stress relaxation experiments were carried out using an ARES (TA Instruments, France) controlled strain rheometer equipped with a plastic cone-and-plate geometry (diameter: 25 mm; angle: 0.0996 rad; truncation: 54 µm) and a Peltier temperature controller. Samples were covered with paraffin oil to prevent evaporation during measurements. Stress relaxation tests were performed for up to 14 h at 37°C and 5% strain (strain rise time of 10 s). The hydrogel formulation used for the general characterization of the rheological properties of wPBA/glucamine hydrogels was composed of 300 kDa HA (DS: HA-wPBA, 24%; HA-glucamine, 32%), with an HA content of 1% (w/v) and a wPBA/glucamine molar ratio of 1:1. Two formulations were then selected and characterized: a "soft hydrogel" formulation, composed of 300 kDa HA (DS: HA-wPBA, 24%; HA-glucamine, 52%), with an HA content of 1% (w/v) and a wPBA/glucamine molar ratio of 1:1; and a "stiff hydrogel" formulation, composed of 100 kDa HA (DS: HA-wPBA, 40%; HA-glucamine, 52%), with an HA content of 2.5% (w/v) and a wPBA/glucamine molar ratio of 1:1.

Stability and biodegradability studies: Hydrogel stability was investigated, either in PBS or serum-containing medium, as previously described.[28] Biodegradability was investigated in PBS, using hyaluronidase (100 $U.mL^{-1}$), as previously described.[28] The reported mass ratio represents the hydrogel mass at a specific time divided by its initial mass.

Biological investigations

Cell culture and encapsulation: L929 murine fibroblast cells were amplified in DMEM medium supplemented with 10% FBS and 1% penicilline/streptomycin. Human ASCs were isolated from lipoaspirates as previously described,[29] and amplified in growth medium supplemented with 1% penicilline/streptomycin. Human ASCs were used between passages 2 and 5. For cell encapsulation, HA-wPBA and HA-glucamine were first separately dissolved in DMEM medium supplemented with 10% FBS and 1% penicilline/streptomycin. Cells were then pelleted and resuspended in the HA-glucamine solution (serum-containing medium) prior to mixing with the HA-wPBA solution (serum-containing medium). The number of resuspended cells, and the volumes of HA-wPBA and HA-glucamine/cells were calculated to obtain the desired final HA content (1% and 2.5% [w/v]) and wPBA:glucamine molar ratio

(1:1), with a final cell density of 10^6 cells.mL^{-1}. The culture medium was changed every 2-3 days.

Viability, metabolic activity and proliferation assays: Cell viability, metabolic activity and DNA content were assessed at day 0, 3 and 7, using LIVE/DEAD™ staining, the CCK-8 assay, and Picogreen™ assay, respectively. For LIVE/DEAD™ staining, hydrogels were formed in an 8-well chamber slide (IBIDI) and incubated with Calcein AM and ethidium homodimer as per manufacturer's recommendations. Images were acquired via confocal microscopy (A1RS, Nikon). Cell viability was calculated as the number of living cells divided by the total cell number (i.e., sum of living and dead cells). Regarding the metabolic activity assay, hydrogels were formed in a 48-well plate and incubated for 2 hours with a CCK-8 solution as per the manufacturer's recommendations. The absorbance at 460 nm of the supernatant was measured (Tristar 2S plate reader, Berthold Technologies), and the results were normalized to the initial absorbance. After the metabolic activity assay, DNA content was assessed using the Picogreen™ assay. Hydrogels were immersed in TE buffer before being frozen at -80 °C overnight. Then, the hydrogels were crushed until complete dissolution, and Picrogreen reagent was added. The fluorescence of the solution was measured (ex: 480 nm, em: 520 nm; Tristar 2S plate reader, Berthold Technologies), and the results were normalized to the initial fluorescence.

Statistical Analysis

All data are shown as mean ± standard deviation. Statistical analysis was carried out using GraphPad to evaluate statistical significance via Student's t-test or one-way ANOVA with Tukey's post hoc test.

Results

Synthesis of boronate ester-based hydrogel precursors

With the aim to screen PBA/diol couples, we selected a large variety of commercially available PBA derivatives and diols, all presenting a primary amine for their straightforward grafting onto HA via amidation (Figure 1a and 1b). Regarding PBA derivatives, we selected the 2PBA, 3PBA, 4PBA, PymBA, PydBA and BX (full names are provided in the material section). Available amino diols were mainly monosaccharide derivatives, including glucosamine, galactosamine, fructosamine, dulcitolamine and glucamine. Tris, aminopropanediol, serinol and dopamine were also investigated. Two additional aminated molecules were synthesized in-house, namely wPBA (Figure S1 and S2) and iditolamine

(Figure S3 and S4). Aminated molecules were grafted onto 300 kDa HA. For the direct comparison of PBA/diol couples, synthetic conditions were systematically optimized to match the DS of the various HA-PBA components, and those of HA-diol components. We successfully synthetized HA-2PBA, HA-4PBA, HA-BX and HA-wPBA at a similar DS of ≈ 24%, as confirmed by ^{1}H NMR or elemental analysis (Figure 1c and S5, and Table S1). Unlike the other HA-PBA syntheses, the synthesis of HA-wPBA in aqueous conditions did not require the addition of 10% (v/v) of DMSO, highlighting the higher hydrophilicity of wPBA as a practical advantage. As a consequence, wPBA also uniquely allowed to reach higher DS (tested up to 60%) without polymer precipitation. HA-3PBA repeatedly precipitated at any DS above 10%, and was therefore not included in the following experiments. We also did not succeed in functionalizing HA with PymBA or PydBA under the selected synthetic conditions; these two molecules were therefore not further investigated. In parallel, we successfully matched the DS of various HA-diol components (i.e., HA-glucosamine, HA-galactosamine, HA-fructosamine, HA-dulcitolamine, HA-glucamine, HA-iditolamine) to ≈ 32%, as confirmed by unreacted amine dosage (TNBS) and elemental analysis (Figure 1c, Table S2 and S3). Other amino diols failed to be grafted onto HA (i.e., tris, aminopropanediol and serinol) or produced unstable precursors (i.e., HA-dopamine), and were therefore not further investigated.

Boronate ester-based hydrogel design

To screen PBA/diol crosslinking couples at physiological pH, all selected HA-PBA and HA-diol components were separately dissolved in PBS at a fixed HA concentration of 1% (w/v), and systematically mixed two-by-two in an equimolar PBA:diol ratio. A preliminary macroscopic observation revealed the unique ability of the wPBA/glucamine couple to form a hydrogel under physiological conditions of pH and temperature, in a quasi-instantaneous manner (Supplementary movie 1). Dynamic shear rheological measurements (frequency sweeps) further suggested the successful formation of a dynamic covalent hydrogel with the newly-identified couple, as indicated by a shear elastic modulus (G' at 1 Hz) of 174 Pa that is 10- to 100-fold higher than that of any of the other PBA/diol combinations (Figure 1d). Unmodified HA was used as a control precursor, and showed no gelation or significant increase in G' with any of the investigated HA-PBA or HA-diol components. This observation excluded the contribution of hydrogen bonding or any unidentified interaction to the observed gelation, further confirming wPBA/glucamine crosslinking.

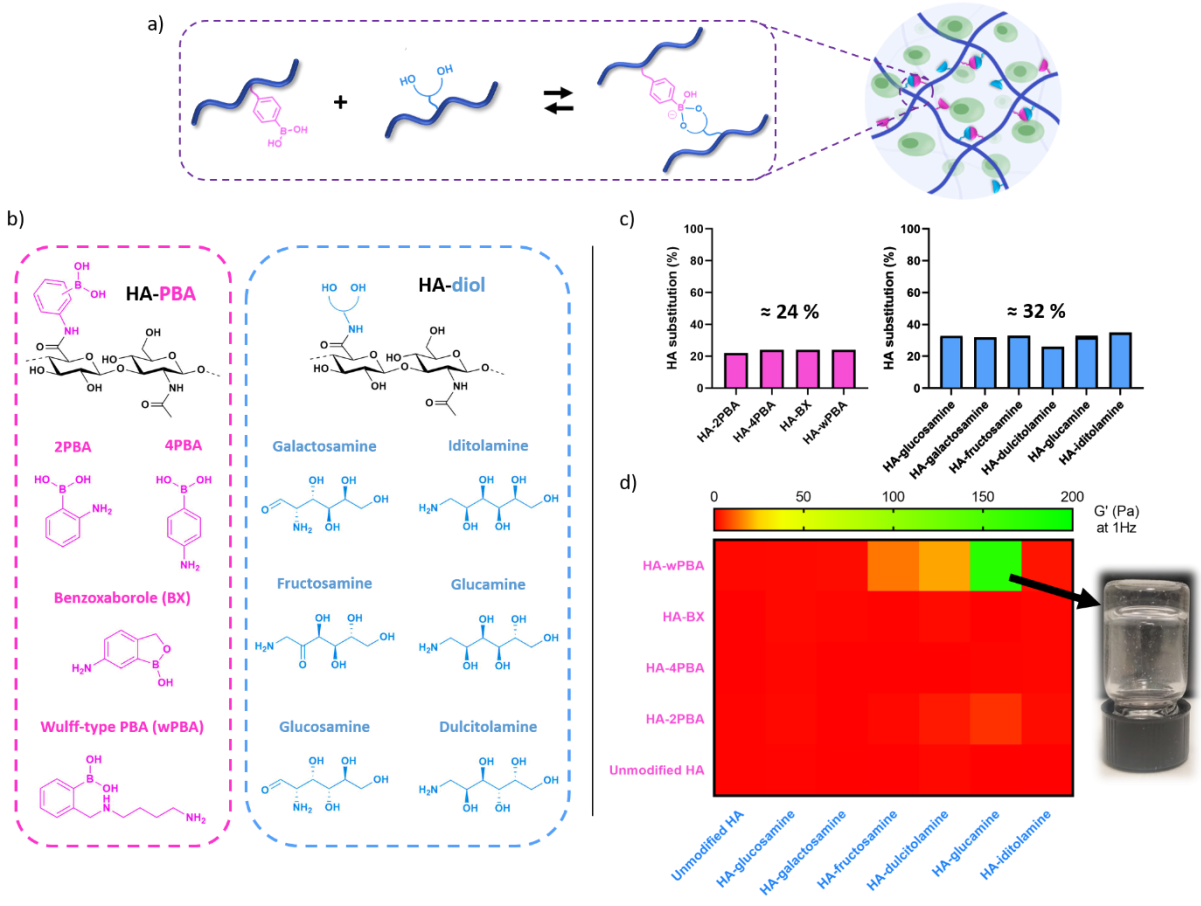

Figure 1. Identification of a new crosslinking couple for the design of boronate ester-based hydrogels under physiological conditions of pH and temeprature. a) Schematic of the reversible reaction between a phenylboronic acid derivative and a diol, which produces boronate ester functions used for dynamic covalent crosslinking. b) Libraries of aminated PBAs (in pink) and amino diols (in blue) investigated to produce hyaluronic acid (HA) hydrogels. c) The matching degrees of substitution (DS) of HA-PBAs (in pink) and HA-diols (in blue), determined by ^{1}H NMR and unreacted amine dosage, respectively. d) Heat map of PBA/diol couple screening, revealing the unique ability of the wPBA/glucamine couple to form a hydrogel at physiological pH. The figure presents the shear storage moduli (G' at 1 Hz) of the various couples, determined via dynamic shear rheology (frequency sweeps) at 37 °C.

The formation of hydrogels, yet much softer, was also observed when mixing HA-wPBA with HA-fructosamine (G' of 19 Pa) or HA-dulcitolamine (G' of 14 Pa). Overall, wPBA was the only PBA derivative that efficiently led to hydrogel formation under physiological conditions of pH and temperature. Interestingly, applying wPBA/glucamine crosslinking to another polysaccharide (i.e., alginate) also led to successful dynamic hydrogel formation (Figure S6), suggesting that wPBA/glucamine is a universal crosslinking couple for dynamic hydrogel design. To our knowledge, this is the first report of the use of wPBA/glucamine as a crosslinking couple to produce boronate ester-based hydrogels under physiological conditions of pH and temperature. This new crosslinking reaction will be the focus of the next sections.

Rheological characterization of wPBA/glucamine-based hydrogels

We first characterized the general rheological properties of wPBA/glucamine hydrogels via dynamic shear rheology, using the same HA hydrogel formulation as in the screening experiment (see method section for formulation details). We confirmed the quasi-instantaneous gelation (within seconds) of the hydrogel, which was indicated by G' (1 Hz) values superior to G'' (1 Hz) values from the beginning of the measurements in a time sweep experiment (Figure 2a). These data also revealed a time to equilibrium of ≈ 10-20 min before reaching plateaus in shear moduli. We then performed frequency sweep experiments to characterize the dynamic covalent nature of the hydrogel. The boronate ester-based hydrogel had the typical frequency-dependent rheological behavior of dynamic covalent hydrogels, which is similar to that of a macromolecular solution composed of a high molecular weight (MW) polymer at a high concentration (Figure 2b).[12,20] More specifically, at low frequencies (i.e., $\omega < 0.05$ Hz), measurement intervals exceeded the crosslinks reorganization time, providing enough time for the hydrogel network to reorganize and dissipate the stored deformation energy, which resulted in an apparent liquid-like behavior ($G' < G''$). Conversely, at high frequencies (i.e., $\omega > 0.5$ Hz), the network no longer had the time to dissipate the energy via crosslinks reorganization within the measurement intervals, exhibiting a solid-like behavior ($G' > G''$). The G'/G'' crossover frequency (ω_c) can be used to estimate hydrogel relaxation time (τ_r), which reflects the time to dissipate the energy upon deformation, where $\tau_r = {}^{1}/_{\omega_c}$.[19,26] The τ_r of the hydrogel was estimated to be of 33 s ($\omega_c \approx 0.03$ Hz), which reflects a fast relaxation compared to other classes of viscoelastic hydrogels, such as ionically crosslinked alginate hydrogels (τ_r = 100-1000 s)[30] and hydrazone-based hydrogels (τ_r = 1000-10000 s).[7,31] Such a fast relaxation translates into high malleability, which is desirable in numerous biomedical applications, including drug/cell delivery.

We then systematically investigated the effects of the HA MW, DS, and content, as well as the wPBA:glucamine molar ratio, on the rheological properties of the hydrogels. The G' value at a fixed frequency of 1 Hz was used as an arbitrary value for comparison (G'' values and raw phase data can be found in Figure S7 and 8). To evaluate the effect of HA MW, we matched the DS of 100 kDa and 300 kDa HA precursors, with wPBA DS of 24% and glucamine DS of 32%. Contrary to 300 kDa HA, 100 kDa HA precursors did not form a hydrogel at an HA concentration of 1% (w/v) and a wPBA:glucamine molar ratio of 1:1. Higher DS (HA-wPBA, 40%; HA-glucamine, 52%) were required to obtain 100 kDa HA-based hydrogels. With similar higher DS (matching crosslinking density of 4.77 mM), 300

kDa HA hydrogels had unexpectedly lower shear elastic moduli (*G′*) than 100 kDa hydrogels (72 vs 140 Pa), suggesting that increasing HA MW could lead to a decrease in the shear elastic modulus of boronate ester-based hydrogels (Figure 2c). Increasing the precursor DS of 300 kDA hydrogels, which increased the crosslinking density from 3.61 mM to 4.77 mM, also counterintuitively led to a lower shear elastic modulus (Figure 2d). Previous reports on purely covalent HA hydrogels have shown that their stiffness (Young's modulus) is mainly independent of HA MW, and that it increases when increasing the crosslinking density.[28] Our data suggest that the relationships between MW, crosslinking density and elastic properties differ between covalent and dynamic covalent HA hydrogels. When increasing HA MW and DS, we observed a noticeable increase in the viscosity of the hydrogel precursor solutions. This may reflect some polymer entanglement, as well as weak interactions between the immobilized wPBA and the vicinal diols of HA, together restricting polymer motion and hindering boronate ester-based crosslinking.

Finally, we investigated the effects of the HA content and wPBA:glucamine molar ratio, which are directly linked to the crosslinking density, on the rheological properties of the hydrogels. 100 kDa HA hydrogels at 1, 2 and 3% (w/v) exhibited shear elastic moduli (*G′* at 1 Hz) of 140 Pa, 659 Pa and 1 267 Pa, respectively, demonstrating that the shear elastic modulus of boronate ester-based hydrogels increases with polymer content (Figure 2e). Experiments on the effect of the wPBA:glucamine molar ratio showed that getting closer to an equimolar ratio, which maximizes the crosslinking density (4.77 mM vs 2.06 mM vs 1.76 mM for the 1:1, 1:4 and 4:1 wPBA:glucamine molar ratios, respectively), maximized *G′* values (140 Pa) (Figure 2f).

Overall, our results confirmed the dynamic nature of the new boronate ester-based hydrogels, as well as their fast relaxation, which reflects malleability. We also showed that their rheological properties are a function of the crosslinking density, but may be altered by the viscosity of the precursor solutions.

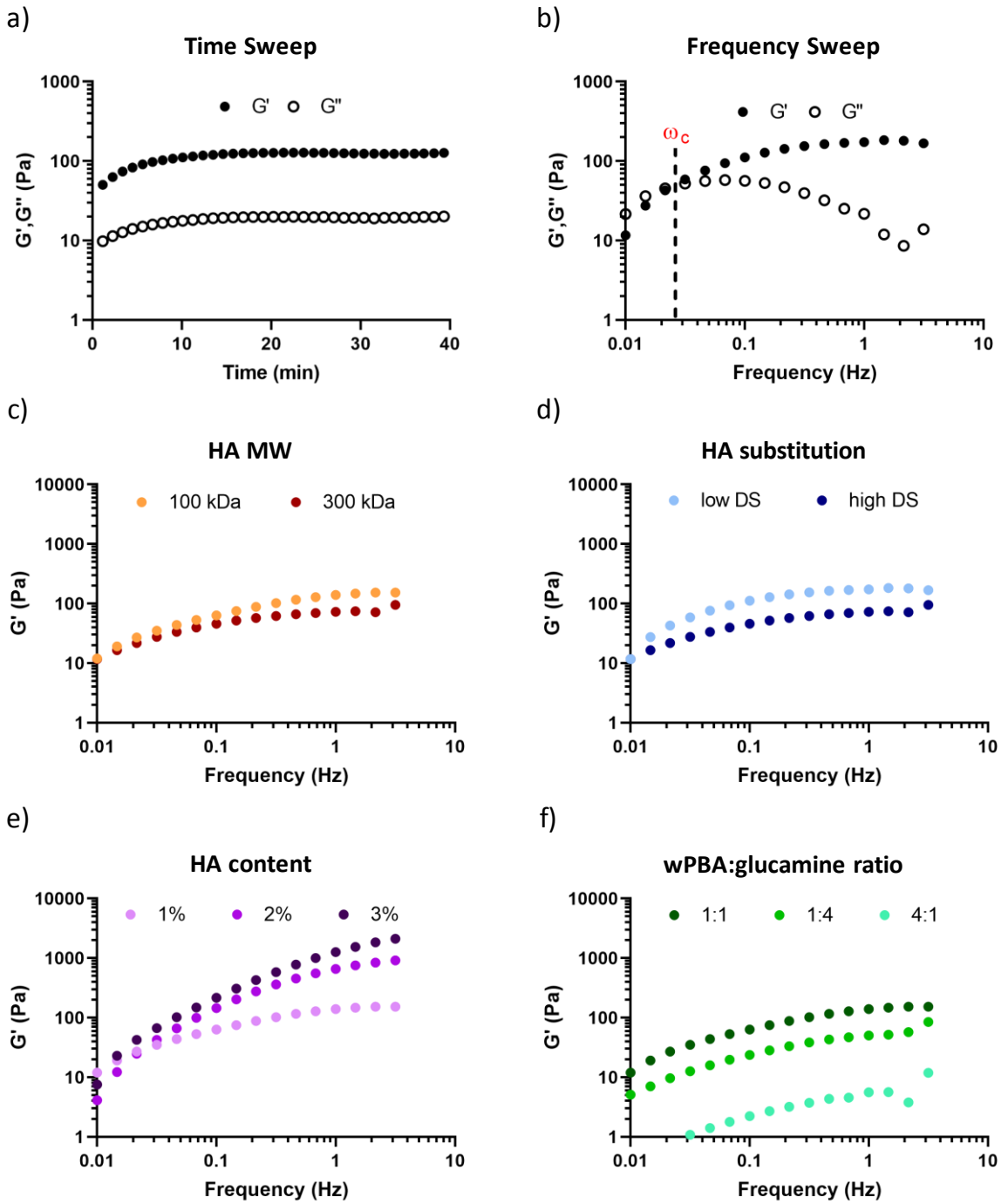

Figure 2. Rheological properties of boronate ester-based hydrogels composed of HA-wPBA and HA-glucamine. a) Time sweep experiment 1% (w/v) 300 kDa HA (DS: HA-wPBA, 24%; HA-glucamine, 32%; equimolar ratio) revealing a quasi-instantaneous gelation, and b) Frequency sweep experiment confirming the dynamic nature of the hydrogel. The influence of c) HA MW, d) HA precursor DS (low substitution: wPBA DS of 24% and glucamine DS of 32%; high substitution: wPBA DS of 40% and glucamine DS of 52%), e) HA content, and f) wPBA:glucamine molar ratio on hydrogel elastic modulus, evaluated using dynamic shear rheology.

Swelling/stability profiles of wPBA/glucamine-based hydrogels

Stability and lack of swelling are two essential features of hydrogels to consider for usability. Due to the dynamic nature of boronate ester crosslinks, which makes them prone to cleavage, producing boronate ester-based hydrogels that are nonswelling and stable over weeks in wet conditions remains a challenge.[12,21,24–26] While some authors used secondary covalent crosslinking to stabilize the hydrogels,[32] this strategy makes the systems more complex, and necessarily alters their viscoelastic properties, therefore affecting their malleability and/or injectability. With the aim to identify nonswelling and stable hydrogel formulations, we systematically investigated the effects of the HA MW, DS, and content, as well as the wPBA:glucamine molar ratio, on the hydrogel swelling and stability. Following overnight stabilization, the hydrogels were immersed in PBS at 37 °C to mimic physiological conditions of pH and temperature, prior to monitoring their mass over time. These experiments provided two pieces of information: the initial degree of shrinking/swelling of the hydrogels after overnight crosslinking stabilization, and their long-term stability in wet conditions.

Comparing hydrogels with matching DS (HA-wPBA, 40%; HA-glucamine:52%), HA content (1% [w/v]), and wPBA:glucamine molar ratio (1:1), we observed that increasing HA MW from 100 to 300 kDa decreased the initial hydrogel shrinking, with mass ratios before immersion of 0.51 ± 0.05 and 0.93 ± 0.04, respectively (Figure 3a). We then evaluated the influence of DS, at a fixed HA content (1% [w/v]) and a fixed molar ratio (1:1), by comparing low DS (HA-wPBA, 24%; HA-glucamine, 32%) and high DS (HA-wPBA, 40%; HA-glucamine, 52%). After overnight stabilization, hydrogels with low DS showed no initial shrinking (mass ratio of 1.01 ± 0.01) while hydrogels with high DS showed some minimal shrinking (mass ratio of 0.93 ± 0.04) (Figure 3b). However, once immersed, only hydrogels with high DS remained stable over 1 month. Hydrogels with low DS gradually swelled over 7 days (up to a mass ratio of 1.72 ± 0.04), before progressively dissolving. As DS is related to the crosslinking density, the swelling of hydrogels with low DS could result from an insufficient crosslinking density to counterbalance osmotic forces. Of note, hypothesizing that the increased stability of high DS hydrogels results mainly from a higher crosslinking density is somewhat incoherent with the slight decrease in their shear elastic modulus previously observed, warranting further mechanistic investigation.

We then evaluated the influence of the polymer content on the swelling of 100 kDa HA hydrogels (high DS), comparing HA contents of 1%, 2% and 3% (w/v). Increasing the polymer content from 1 to 3% (w/v) led to reduced initial shrinking, with mass ratios of

0.51 ± 0.05 and 1.00 ± 0.01, respectively (Figure 3d). We observed a similar trend with 300 kDa HA hydrogels (Figure S9). This increase in initial swelling (or reduced shrinking) with increased HA concentration could be attributed to the hydrophilicity of HA that induces osmotic forces, as previously reported.[10,33] Regarding stability, all three hydrogels showed minimal variations in mass over 1 month.

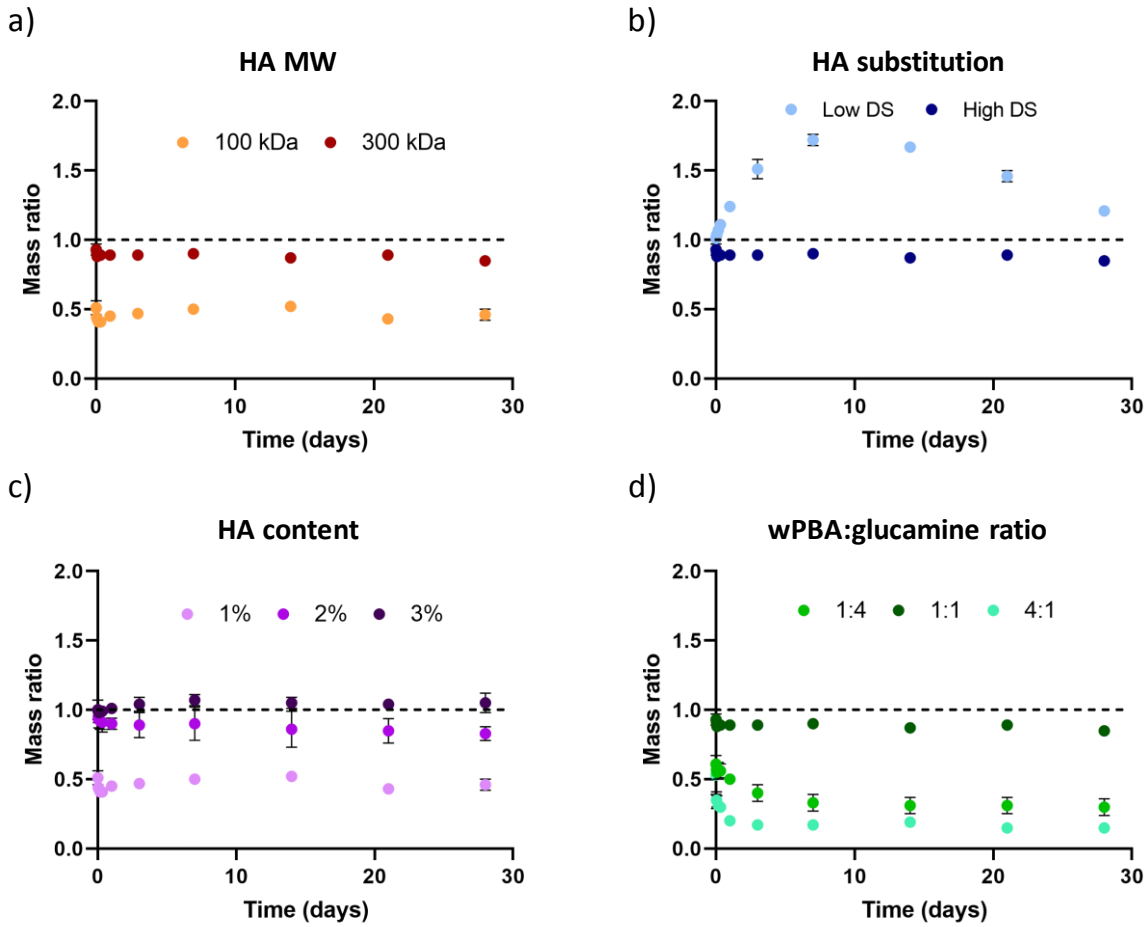

Figure 3. Swelling and stability characteristics of boronate ester-based HA hydrogels. The influence of a) HA MW, b) HA DS, c) HA content, and d) wPBA:glucamine molar ratio on hydrogel stability/swelling behavior. Results on HA DS compare low DS (HA-wPBA, 24%; HA-glucamine, 32%) and high DS (HA-wPBA, 40%; HA-glucamine, 52%). Data are shown as mean ± SD (n = 3).

Finally, we investigated the influence of the wPBA:glucamine molar ratio on the swelling/stability properties. Our results revealed the unexpected importance of the use of an equimolar ratio for the formation of hydrogels that do not considerably shrink. After overnight stabilization, at a fixed total HA concentration (1% [w/v]), an excess of any of the two reactive molecules (i.e., wPBA:glucamine molar ratio of 1:4 or 4:1) led to important hydrogel shrinking (mass ratios of 0.61 ± 0.02 and 0.53 ± 0.14, respectively). On the contrary, the hydrogel formulation with an equimolar ratio showed minimal shrinking (mass ratio of

0.93 ± 0.04) (Figure 3e). When forming hydrogels with 2 components, getting closer to an equimolar ratio of reactive functions at a fixed total polymer content mathematically maximizes the crosslinking density, further suggesting a potential role of the crosslinking density on the general swelling behavior of boronate ester-based hydrogels. However, the exact mechanism behind the influence of the wPBA:glucamine molar ratio on the swelling/stability properties of these hydrogels remains to be elucidated.

Overall, most of the wPBA/glucamine hydrogel formulations that we investigated were stable long term under physiological conditions of pH and temperature, and some of them had minimal to no initial shrinking. No direct correlation between crosslinking density and swelling/shrinking could be identified (Figure S10); and the competing influences of the different parameters remain difficult to unravel, calling for further fundamental mechanistic investigations.

Optimization of stable and nonswelling boronate ester-based hydrogels

Based on these investigations, we designed two boronate ester-based hydrogel formulations, which we named "soft" and "stiff". The soft hydrogel formulation was obtained by taking advantage of the unique ability of high MW HA (300 kDa) to form a hydrogel at low DS and low polymer content (1% w/v); while the stiff hydrogel used 100 kDa HA, which reached higher G' values in our previous experiments and allowed us to increase the polymer content to 2.5% (w/v). DS and polymer contents were carefully selected to balance each other out in order to avoid shrinking and swelling phenomena (see method section for further formulation details). We showed that the soft and stiff hydrogels are both nonswelling and stable over at least two months, with shear elastic moduli (G' at 1 Hz) of 132 ± 12 Pa and 1035 ± 73 Pa, respectively (Figure 4a, c and d). The two hydrogels are also stable in serum-containing medium (i.e., DMEM with 10% FBS), with swelling/stability profiles similar to those of hydrogels prepared in PBS. To our knowledge, this is the first report of boronate ester-based hydrogels that are nonswelling and stable long term in vitro. Using accelerated conditions of enzymatic degradation (i.e., hyaluronidase treatment), we confirmed that these HA hydrogels are biodegradable, with distinct degradation rates: the soft hydrogel was degraded within one day, while the stiff hydrogel reached complete degradation after two weeks (Figure 4b). The two formulations exhibited specific frequency-dependent profiles, and only the stiff formulation had a G'/G'' crossover observable in the investigated range of frequency (0.01-5 Hz). The τ_r of the stiff formulation (ω_c = 0.04 Hz) was calculated to be 25 s, while that of the soft formulation exceeded 100 s (ω_c < 0.01 Hz). To further characterize the relaxation time of

the two hydrogels, we performed direct stress relaxation tests. The soft and stiff hydrogels showed complete stress relexation, and had half relaxation times ($\tau_{r1/2}$) of 2 and 0.7 s, respectively (Figure 4d). These experiments showed times to complete relaxation of ≈ 44 s and ≈ 131 s, for the soft and stiff hydrogels, respectively, in the same range as those obtained in the frequency sweep experiments. For dynamic covalent hydrogels, relaxation time is believed to be intrinsically related to the crosslinking mechanism, at the molecular level.[34] However, despite the use of the same dynamic crosslinking reaction, the two hydrogels differed in their relaxation times. The design of the soft and stiff hydrogels required the use of distinct HA MWs (300 kDa and 100 kDa, respectively) and polymer contents (1% and 3% [w/v], respectively), indicating a possible role of these two parameters in the relaxation time, as previously suggested.[30]

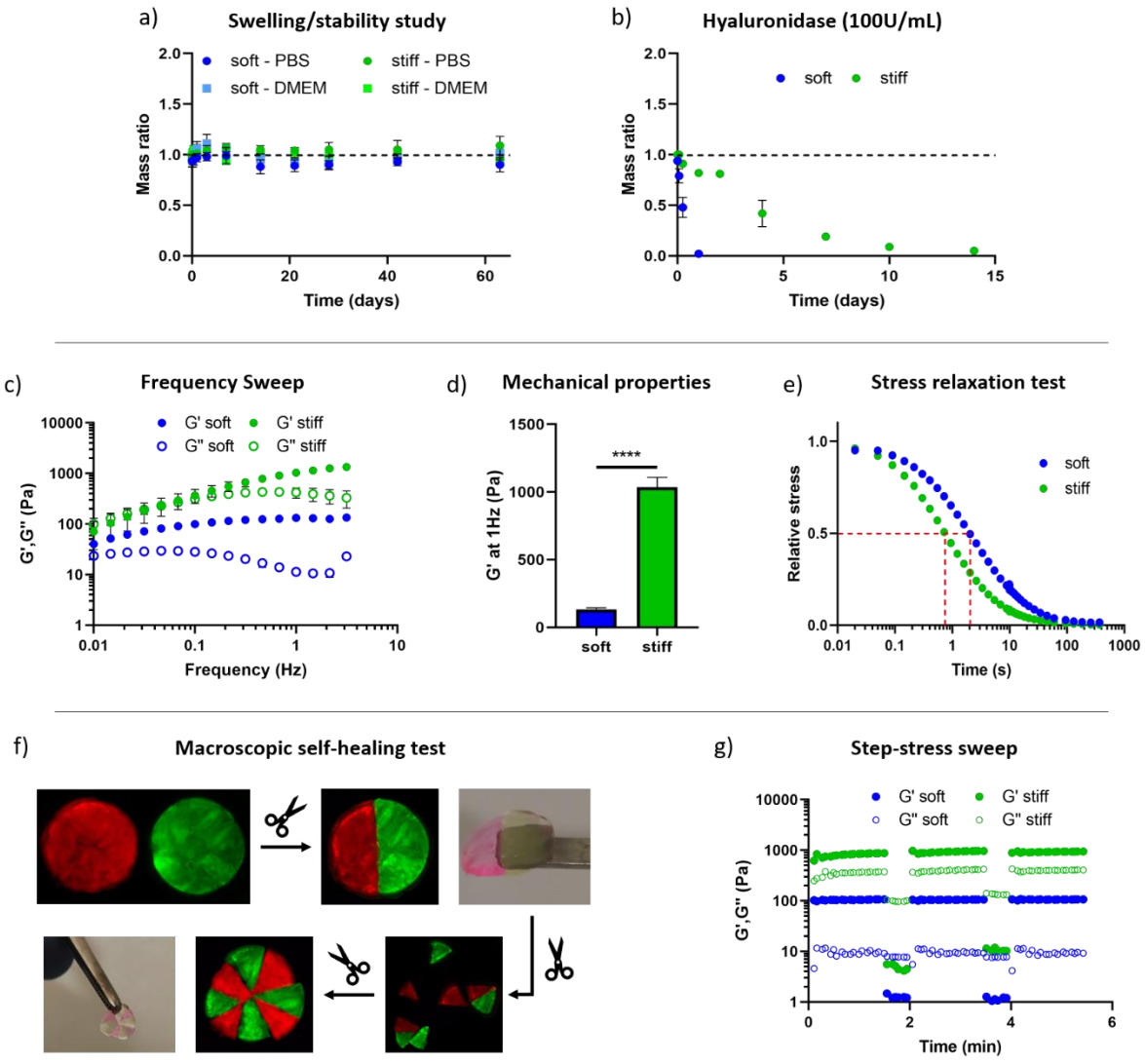

Figure 4. Design of nonswelling and stable boronate ester-based hydrogels, with distinct rheological properties. a) Stability study of the soft and stiff hydrogels immersed in PBS or culture medium,

confirming that they are nonswelling and stable long term. b) Enzymatic degradation study (hyaluronidase, 100 $U.mL^{-1}$) of the soft and stiff hydrogels, showing degradation in one day and two weeks, respectively. Data are shown as mean ± SD (n = 3). c) Frequency sweep experiments on the soft and stiff hydrogels, and d) the obtained shear elastic moduli (G') at 1Hz. Data are shown as mean ± SD (n = 3). e) Relaxation tests, confirming the fast relaxation of the two hydrogels. f) Macroscopic and g) rheological confirmation of the self-healing properties of the two dynamic hydrogels after network disruption.

Dynamic covalent crosslinking mechanisms, where covalent bonds are continuously forming and breaking, are known to produce hydrogels with self-healing properties.[35] To confirm the self-healing capacity of the new boronate ester-based hydrogels, we prepared two discs of fluorescently-labelled hydrogels with distinct colors, cut them into halves, before recomposing a hydrogel disc with a piece of each (Figure 4f). After 5 minutes, the recomposed hydrogel could be lifted and was able to support its own weight. The healed hydrogel could be further cut into fragments and reassembled into a single hydrogel. To further demonstrate the self-healing property, we performed a step-stress sweep test, through oscillatory shear cycles of alternated low (1 Pa) and high (1200 Pa) stress. When a high stress was applied, G' values of both hydrogels dropped of several orders of magnitude, below the G'' values, as an indication of network disruption (Figure 4g). Switching back to low stress led to the instantaneous recovery of the initial G' values of the hydrogels, indicative of rapid self-healing. An additional measurement of the G' and G″ values of a manually crushed hydrogel (soft formulation) further confirmed the expected self-healing properties of the new boronate ester-based hydrogels (Figure S11).

Cytocompatibility of boronate ester-based hydrogels

As a preliminary experiment, we first evaluated the impact of the use of culture medium on the rheological properties of a boronate ester-based hydrogel (i.e., soft formulation) using three common cell culture media, namely DMEM, RPMI and Promocell. We observed that switching from PBS to culture medium had minimal impact on their properties overall, but could induce a slight increase in their shear elastic modulus in a culture medium-dependent manner, suggesting some interactions with medium components that are yet to be deciphered (Figure S12). To evaluate the cytocompatibility of wPBA/glucamine hydrogels, we then assessed the viability (live/dead staining), metabolic activity (CCK-8 assay) and DNA content (Picogreen assay) of encapsulated murine L929 fibroblast cells (following ISO recommendations for cytocompatibility validation) and hASCs (Figure 5a). For both hydrogel formulations, encapsulated L929 cells had a viability of > 95% over 7 days (Figure 5b). Confocal imaging at day 7 showed the presence of numerous cell clusters, suggesting cell proliferation within the hydrogels, which is commonly observed with proliferative cell

lines.[36] CCK-8 assays corroborated this observation, with 17.2 ± 0.3-fold and 13.9 ± 0.2-fold increases (relative to day 0) in cell metabolic activity at day 7, for the soft and stiff hydrogels, respectively (Figure 5c). Regarding the DNA content, it increased to 411% ± 127% of the initial value over 7 days in soft hydrogels, while its increase in stiff hydrogels was not significant (Figure 5d). This difference may be the result of the higher elastic modulus and polymer content of the stiff hydrogels, which may increase cell confinement and thus limit cell proliferation.[2] Similar biological investigations were then performed on encapsulated hASCs. Live/dead staining and confocal imaging revealed a high cell viability (> 95%) over 7 days in the two hydrogels (Figure 5e). Over the 7-day experiment, the metabolic activity and DNA content of encapsulated hASCs remained constant in the stiff hydrogels, while both biological readouts revealed a slight but significant increase in the soft hydrogels (relative values of 161% ± 15% and 125.8% ± 6.7%, respectively). These results suggest a modest proliferation of the encapsulated hASCs (Figure 5f and g). We previously observed a similar limited proliferation of hASCs in other HA hydrogels, which can be related to a lack of a specific stimulus (e.g., proliferation or differentiation medium) and/or adhesive motifs in the hydrogels.[37] Finally, we confirmed that cells were homogenously distributed throughout the hydrogels, as evidenced by similar relative cell number in each hydrogel section (Figure S13). Overall, using cell types of two different origins (murine vs human) and three biological readouts, we showed that the newly developed hydrogels are cytocompatible and can be used for 3D cell culture.

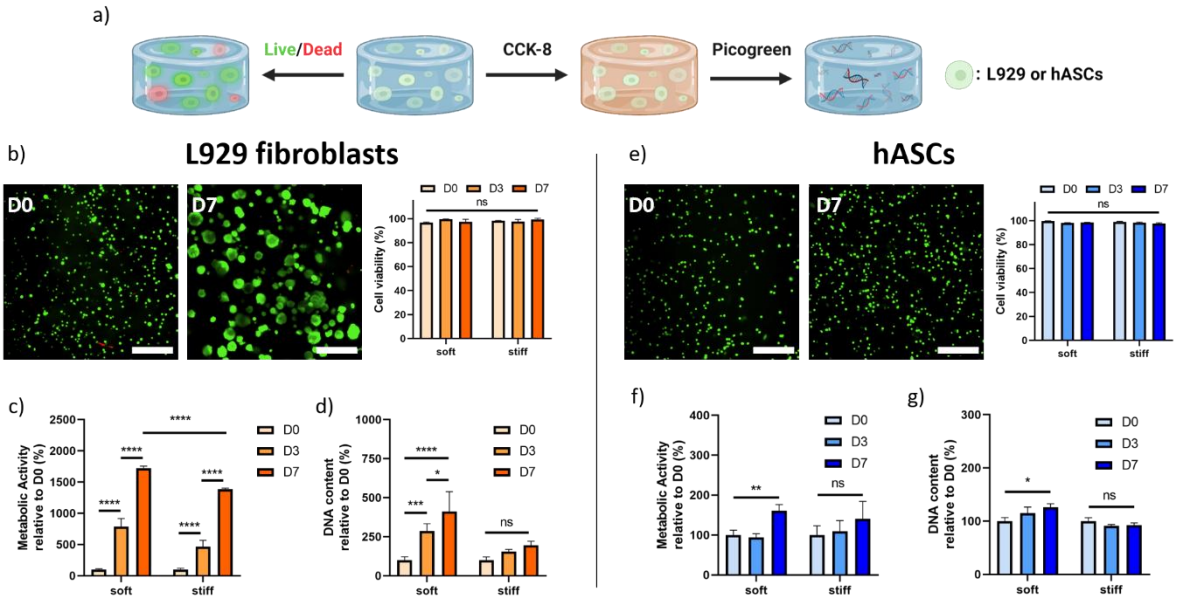

Figure 5. Cytocompatibility of the soft and stiff boronate ester-based hydrogels. a) The viability of two cell types (L929 fibroblasts and hASCs) was assessed using three distinct methods: Live/Dead staining, metabolic assay (CCK-8), and DNA quantification (Picogreen). b) Representative stack

views of L929 cells encapsulated in soft hydrogels, and the evaluation of their viability in the soft and stiff hydrogels (scale bar = 300 µm). c) Metabolic activity and d) DNA content of L929 encapsulated in the two hydrogels, monitored over 7 days of culture. e) Representative stack views of hASCs encapsulated in soft hydrogels, and the evaluation of their viability in the soft and stiff hydrogels (scale bar = 300 µm). f) Metabolic activity and g) DNA content of hASCs encapsulated in the two hydrogels, monitored over 7 days of culture. Data are shown as mean ± SD (n = 4) with statistical significance determined using one-way ANOVA with a Tukey's post hoc test (ns : not significant, *p < 0.05, **p < 0.01, ***p < 0.001 and ****p < 0.0001).

Discussion

Boronate ester formation is one of the few dynamic covalent reactions identified to date for the design of viscoelastic hydrogels.[4,5] Compared to crosslinking via Schiff base formation (e.g., imine, hydrazone, oxime), which has been extensively studied,[1,7] boronate ester crosslinking and its use in biomedical applications remain marginal, possibly suffering from a general lack of efficiency at physiological pH. In this study, we showed that combining wPBA and glucamine is a convenient way to produce dynamic hydrogels under physiological conditions. More importantly, among all of the investigated combinations, only the wPBA/glucamine couple presented the necessary binding affinity to produce HA hydrogels (with the possible exception of the combination of wPBA with dulcitolamine or fructosamine). While the exact mechanism behind boronate ester formation is still debated in some aspects, it is now recognized that it is strongly influenced by (i) the pKa of the boronic acid, and (ii) the reactivity of the diol toward the boronic acid.[16,38,39]

A boronic acid exists under a neutral form and an anionic form (boronate), both in ionic equilibrium (with a typical pKa of ≈ 9). Due to its tetrahedral (sp^3) hybridization, the boronate ion is more stable and considered less reactive toward diols than the neutral form. Accordingly, the esterification process is believed to happen preferentially through the addition of diols on the trigonal (sp^2) boronic acid, to form an unstable boronic ester (sp^2).[16] Boronic ester formation generates ring strain, thus favoring hybridization into a more stable, tetrahedral boronate ester (sp^3). As such, the pKa of a boronic ester is lower than that of the corresponding boronic acid.[16,38] Yet, it is often not low enough to favor boronate ester formation at physiological pH. Decreasing the pKa of a boronic acid, and therefore decreasing that of the corresponding boronic ester, is one possible approach to favor boronate ester formation at physiological pH. To date, two classes of boronic acid derivatives with low pKa values have attracted particular attention: BX (pKa = 7.2) and wPBA (pKa = 5.5).[38,40] The decreased pKa of BX is the result of the ring strain induced by the intramolecular B-O coordination, which is released upon conversion from an sp^2 to an sp^3 structure, and therefore favors the anionization. As for wPBA, the reduced pKa is attributed to the proximity of the

positively charged ammonium ion from the *o*-aminomethyl group.[41] More specifically, it has been suggested that the *o*-aminomethyl group favors boronate ester formation through an intramolecular mechanism (i.e., loose-bolt postulate), where an inserted solvent molecule is lost, temporarily generating a reactive intermediate (i.e., trigonal boronic acid) that promotes diol complexation.[41] In our study, both BX and wPBA were tested. wPBA is the only boronic acid derivative that showed appreciable interactions with diols at physiological pH, confirming the potential of PBAs with a low pKa to promote effective binding and crosslinking. We also showed that the water solubility of wPBA advantageously allows to reach higher crosslinking density, favoring hydrogel formation and stability. Interestingly, none of the investigated combinations with BX led to hydrogel formation, suggesting much lower binding affinities, and further advocating for the use of wPBA. However, this observation goes against a previous study that convincingly demonstrated effective crosslinking when combining BX and fructosamine,[42] possibly calling for further investigations.

Beyond the role of sp^2 to sp^3 conversion, effective boronate ester formation is also strongly influenced by the structure of the diol, which is translated into a binding affinity and a measurable association constant.[16,43] The main improving factor for a higher association constant is the presence of a 1,2-*cis* or 1,3-*cis* diol, ideally in a coplanar conformation.[43] Typically, the catechol group was shown to have one of the highest association constant (830 M^{-1}),[43] which is attributed to its coplanar vicinal diol. In this regard, we tried to functionalized HA with dopamine, a molecule that displays both a catechol group and a primary amine for straightforward immobilization onto HA. Unfortunately, we did not succeed in obtaining HA-dopamine with satisfactory DS and stability as a consequence of the well-described catechol oxidation.[44] Commercially available polyols are almost exclusively monosaccharide derivatives. However, natural monosaccharides (e.g., glucose, galactose, fructose) have relatively low abundance of *cis*-diols, which are mostly present under the minor furanose form of the monosaccharides (abundance ranging from 0.14% to 25%).[45] This translates into low binding affinities, in the range of 4.6 M^{-1} to 160 M^{-1}.[43] Among the natural monosaccharides, fructose has the highest abundance of furanose (25%) and thus the highest affinity toward boronic acid (160 M^{-1}).[45] This supports the fact that, in our study, fructosamine was the only monosaccharide to allow, to some degree, gelation with wPBA. We also investigated a series of amino alditols, which are reduced aminosugars differing only in their stereochemical configurations, including dulcitolamine (2*S*, 3*R*, 4*S*, 5*R*), glucamine

(2*S*, 3*R*, 4*R*, 5*R*), and iditolamine (2*S*, 3*R*, 4*R*, 5*S*). Among them, only the use of glucamine, which corresponds to an aminated sorbitol, led to effective gelation, which was observed only with wPBA. This clearly highlights a specific interaction between wPBA and glucamine, independent of any 1,2-*cis* or 1,3-*cis* diol, based on the particular stereochemical configuration of glucamine. These results also echo the relatively high binding affinity of sorbitol toward PBAs.[43] Interestingly, the sequence of asymmetric carbons (2*S*, 3*R*, 4*R*, 5*R*) of sorbitol and glucamine is similar to that of glucono-δ-lactone, which was recently shown to allow gelation in combination with 4PBA,[34] Fluoro-PBA,[20] BX,[17] and wPBA.[34] However, while an extensive NMR study has shown that a series of three specific hydroxyl groups of sorbitol (i.e., C2, C3, and C5) are involved in boronate ester formation,[46] a different binding site of glucono-δ-lactone was suggested by others.[34] Thus, although beyond the scope of this study, the specific mechanism of boronate ester formation between wPBA and glucamine remains to be elucidated. A recent study showed an important discrepancy between the measured binding affinity of small molecules and actual macromolecular crosslinking,[26] calling for caution in such investigation.

Over the last decade, several PBA/diol couples have been proposed for the design of dynamic covalent hydrogels.[17–21,26] Yet, none of the reported systems was shown to be nonswelling and stable long term. In particular, boronate ester-based hydrogels made of PEG either showed rapid degradation (within hours)[21,26] or required complementary covalent crosslinking for stabilization.[19] We demonstrated that optimized wPBA/glucamine hydrogels made of HA are nonswelling and stable under culture conditions. While a specific binding affinity between wPBA and glucamine cannot be fully excluded, it is possible that the use of HA as a polymer backbone favored the stabilization of the dynamic hydrogels owing to the great number of reactive functions per polymer chain compared to telechelic polymers such as PEG. The physicochemical characterization of the newly-developed system left some grey area and open questions, including the mechanisms behind the influence of the HA MW and concentration on the formation, shrinking, and rheological properties of the hydrogels. More generally, despite a variety of PBA/diol couples proposed to date, boronate ester-based hydrogels still only offer limited ranges of elastic properties (G' of 100 to 1000 Pa) and relaxation times (within tens of seconds). More work is therefore needed to expand their rheological properties, which will almost inevitably include computational modeling to fully unravel the relationship between PBA/diol interactions and the resulting hydrogel properties.

Conclusion

Based on a wide screening of molecules, we identified a new boronic acid/diol couple, namely wPBA and glucamine, with the ability to form dynamic covalent HA-based hydrogels under physiological conditions of pH and temperature. After careful investigation of the physicochemistry of this new system, we were able to produce two HA-based hydrogels that are nonswelling and stable over at least 2 months in culture medium, with distinct shear elastic moduli. We further confirmed their viscoelastic behavior and fast relaxation, as well as their cytocompatibility. These new dynamic covalent HA-based hydrogels could be used in a variety of biomedical applications, ranging from 3D cell culture and bioprinting, to the minimally-invasive delivery of drugs and therapeutic cells.

Acknowledgements

The authors are grateful to the Fondation de l'Avenir pour la Recherche Médicale Appliquée (AP-RM-18-005; CLV), the Fondation pour la Recherche Médicale (ARF201809007012; VD), the Nantes Excellence Trajectory program (NExT Junior Talent 2018, VD; NexT IIP Shelby 2018, CLV), and the Marie-Sklodowska Curie Actions (BABHY-CART project, GAP-846477; VD) for their financial support. They also acknowledge the IBISA MicroPICell facility (Biogenouest), member of the national infrastructure France-Bioimaging supported by the French national research agency (ANR-10-INBS-04), and Denis Loquet at the CEISAM laboratory (Nantes, FRANCE) for their technical support in confocal microscopy and elemental analysis, respectively. The synthesis of wPBA precursor in this project was implemented by the IBISA core facility CHEM-Symbiose, as part of the Biogenouest network.This work also includes NMR experiments carried out on the CEISAM NMR platform.

Conflicts of interest

The authors declare no conflict of interest.

Author contributions

The following author contributions were identified based on the guidelines from CRediT (Contributor Roles Taxonomy). NL contributed to the entire scientific process, from the conceptualization, methodology, and investigation, to the writing. The project was led by VD, who contributed to the conceptualization, methodology, supervision, project administration, and writing. BH, FL and CJ contributed to the resources. LT, PT and MR contributed to the investigation. LT, PT, JJH and GV contributed to the conceptualization. LT, PT, JJH, GV,

MR, CG and AT contributed to the methodology. DS, YV, JL, JG and CLV contributed to the supervision. JJH, CG, AT, JG and CLV contributed to the writing (review and editing).

References

[1] H. Wang, S. C. Heilshorn, *Adv. Mater.* **2015**, *27*, 3717.

[2] O. Chaudhuri, J. Cooper-White, P. A. Janmey, D. J. Mooney, V. B. Shenoy, *Nature* **2020**, *584*, 535.

[3] Z. Tong, L. Jin, J. M. Oliveira, R. L. Reis, Q. Zhong, Z. Mao, C. Gao, *Bioact. Mater.* **2021**, *6*, 1375.

[4] L. Teng, Y. Chen, Y. G. Jia, L. Ren, *J. Mater. Chem. B* **2019**, *7*, 6705.

[5] M. J. Webber, M. W. Tibbitt, *Nat. Rev. Mater.* **2022**, *7*, 541.

[6] C. Loebel, C. B. Rodell, M. H. Chen, J. A. Burdick, *Nat. Protoc.* **2017**, *12*, 1521.

[7] B. M. Richardson, D. G. Wilcox, M. A. Randolph, K. S. Anseth, *Acta Biomater.* **2019**, *83*, 71.

[8] X. Wu, C. He, Y. Wu, X. Chen, *Biomaterials* **2016**, *75*, 148.

[9] S. Kirchhof, F. P. Brandl, N. Hammer, A. M. Goepferich, *J. Mater. Chem. B* **2013**, *1*, 4855.

[10] L. J. Smith, S. M. Taimoory, R. Y. Tam, A. E. G. Baker, N. Binth Mohammad, J. F. Trant, M. S. Shoichet, *Biomacromolecules* **2018**, *19*, 926.

[11] C. C. Deng, W. L. A. Brooks, K. A. Abboud, B. S. Sumerlin, *ACS Macro Lett.* **2015**, *4*, 220.

[12] Y. Chen, D. Diaz-Dussan, D. Wu, W. Wang, Y. Y. Peng, A. B. Asha, D. G. Hall, K. Ishihara, R. Narain, *ACS Macro Lett.* **2018**, *7*, 904.

[13] S. H. Hong, S. Kim, J. P. Park, M. Shin, K. Kim, J. H. Ryu, H. Lee, *Biomacromolecules* **2018**, *19*, 2053.

[14] R. Guo, Q. Su, J. Zhang, A. Dong, C. Lin, J. Zhang, *Biomacromolecules* **2017**, *18*, 1356.

[15] M. Dowlut, D. G. Hall, *J. Am. Chem. Soc.* **2006**, *128*, 4226.

[16] J. A. Peters, *Coord. Chem. Rev.* **2014**, *268*, 1.

[17] T. Figueiredo, V. Cosenza, Y. Ogawa, I. Jeacomine, A. Vallet, S. Ortega, R. Michel, J. D. M. Olsson, T. Gerfaud, J. G. Boiteau, J. Jing, C. Harris, R. Auzély-Velty, *Soft Matter* **2020**, *16*, 3628.

[18] D. Wu, W. Wang, D. Diaz-Dussan, Y. Y. Peng, Y. Chen, R. Narain, D. G. Hall, *Chem. Mater.* **2019**.

[19] S. Tang, H. Ma, H. C. Tu, H. R. Wang, P. C. Lin, K. S. Anseth, *Adv. Sci.* **2018**, *5*, 1.

[20] V. Yesilyurt, M. J. Webber, E. A. Appel, C. Godwin, R. Langer, D. G. Anderson, *Adv. Mater.* **2016**, *28*, 86.

[21] B. Marco-Dufort, J. Willi, F. Vielba-Gomez, F. Gatti, M. W. Tibbitt, *Biomacromolecules* **2021**, *22*, 146.

[22] D. Tarus, E. Hachet, L. Messager, B. Catargi, V. Ravaine, R. Auzély-Velty, *Macromol. Rapid Commun.* **2014**, *35*, 2089.

[23] Y. Wu, J. Wang, L. Li, X. Fei, L. Xu, Y. Wang, J. Tian, Y. Li, *J. Colloid Interface Sci.* **2021**, *584*, 484.

[24] X. Deng, R. Attalla, L. P. Sadowski, M. Chen, M. J. Majcher, I. Urosev, D. C. Yin, P. R. Selvaganapathy, C. D. M. Filipe, T. Hoare, *Biomacromolecules* **2018**, *19*, 62.

[25] J. Lee, J. H. Ko, K. M. Mansfield, P. C. Nauka, E. Bat, H. D. Maynard, *Macromol. Biosci.* **2018**, *18*, 1.

[26] Y. Xiang, S. Xian, R. C. Ollier, S. Yu, B. Su, I. Pramudya, M. J. Webber, *J. Control. Release* **2022**, *348*, 601.

[27] B. Pribulová, M. Petrušová, H. Smrtičová, L. Petruš, *Carbohydr. Res.* **2012**, *363*, 62.

[28] V. Delplace, P. E. B. Nickerson, A. Ortin-Martinez, A. E. G. Baker, V. A. Wallace, M. S. Shoichet, *Adv. Funct. Mater.* **2020**, *30*, 1.

[29] C. Merceron, S. Portron, C. Vignes-Colombeix, E. Rederstorff, M. Masson, J. Lesoeur, S. Sourice, C. Sinquin, S. Colliec-Jouault, P. Weiss, C. Vinatier, J. Guicheux, *Stem Cells* **2012**, *30*, 471.

[30] O. Chaudhuri, L. Gu, D. Klumpers, M. Darnell, S. A. Bencherif, J. C. Weaver, N. Huebsch, H. P. Lee, E. Lippens, G. N. Duda, D. J. Mooney, *Nat. Mater.* **2016**, *15*, 326.

[31] M. Cantini, H. Donnelly, M. J. Dalby, M. Salmeron- Sanchez, *Adv. Healthc. Mater.* **2020**, *9*, 1901259.

[32] S. Tang, H. Ma, H. Tu, H. Wang, P. Lin, K. S. Anseth, *Adv. Sci.* **2018**, *5*, 1800638.

[33] C. B. Rodell, N. Dusaj, C. B. Highley, J. A. Burdick, *Adv. Mater.* **2016**, *28*, 8419.

[34] B. Marco-Dufort, R. Iten, M. W. Tibbitt, *J. Am. Chem. Soc.* **2020**, *142*, 15371.

[35] P. Bertsch, M. Diba, D. J. Mooney, S. C. G. Leeuwenburgh, *Chem. Rev.* **2022**.

[36] K. Flegeau, C. Toquet, G. Rethore, C. d'Arros, L. Messager, B. Halgand, D. Dupont, F. Autrusseau, J. Lesoeur, J. Veziers, P. Bordat, A. Bresin, J. Guicheux, V. Delplace, H. Gautier, P. Weiss, *Adv. Healthc. Mater.* **2020**, *9*, 1.

[37] V. Delplace, N. Lagneau, B. Halgand, F. Loll, J. Guicheux, C. Le Visage, *Tissue Eng. - Part A* **2022**, *28*, S146.

[38] B. M. Dufort, M. W. Tibbitt, *Mater. Today Chem.* **2019**, *12*, 16.

[39] M. Van Duin, J. A. Peters, A. P. G. Kieboom, H. Van Bekkum, *Tetrahedron* **1984**, *40*, 2901.

[40] D. G. Hall, *Boronic Acids: Preparation and Applications in Organic Synthesis and Medicine*, Vol. 53, **2005**.

[41] X. Sun, B. M. Chapin, P. Metola, B. Collins, B. Wang, T. D. James, E. V. Anslyn, *Nat. Chem.* **2019**, *11*, 768.

[42] T. Figueiredo, J. Jing, I. Jeacomine, J. Olsson, T. Gerfaud, J. Boiteau, C. Rome, C. Harris, R. Auzely, *Biomacromolecules* **2019**.

[43] G. Springsteen, B. Wang, *Tetrahedron* **2002**, *58*, 5291.

[44] E. Herlinger, R. F. Jameson, W. Linert, *J. Chem. Soc. Perkin Trans. 2* **1995**, 259.

[45] X. Wu, Z. Li, X. X. Chen, J. S. Fossey, T. D. James, Y. B. Jiang, *Chem. Soc. Rev.* **2013**, *42*, 8032.

[46] J. C. Norrild, *J. Chem. Soc. Perkin Trans. 2* **2001**, 719.

Supplementary information

Synthesis of wPBA

General synthetic pathway

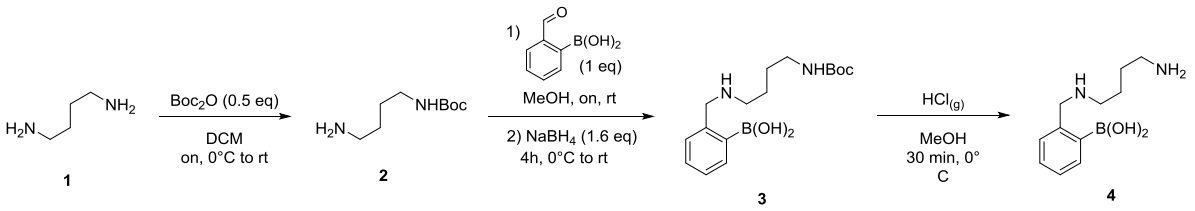

Reagents, solvents and reaction conditions

Di-tert-butylcarbonate (Boc_2O), 1.4-diaminobutane, sodium tetraborohydride ($NaBH_4$) were all provided by Acros-Fisher. 2-(Formyl)phenylboronic acid and methanol (MeOH) were respectively supplied by Apollo Scientific and Merck (Darmstadt, Germany). Sulfuric acid (H_2SO_4) and sodium chloride (NaCl) were provided by VWR. The MB SPS-800-dry solvent system was used to dry dichloromethane. The reactions were carried out in glassware vessels which were either flame dried under vacuum or placed under argon stream for several minutes. Reactions were also performed under rigorous anhydrous conditions and argon stream/positive pressure of argon. Flash column chromatography was carried out using automatic Reveleris Büchi apparatus. Silica cartridges (4 g till 330 g, Büchi) were used with high purity grade of silica (40 µm).

Reaction monitoring and characterisation

All reactions were monitored by TLC on commercially available precoated plates (Kieselgel 60 F254), and the compounds were visualized with $KMnO_4$ solution [$KMnO_4$ (3 g), K_2CO_3 (20 g), NaOH (5% aq.; 5 mL), H_2O (300 mL)] and heating or by UV (254 nm) when possible.

Intermediate and final products were characterised by ^1H and ^{13}C NMR as well as ESI-TOF-HRMS.

NMR studies

Intermediate and final products were characterised by ^1H and ^{13}C NMR. Spectra were recorded on a Bruker Avance 300 spectrometer fitted with a 5 mm i.d. BBO probe carefully tuned to the recording frequency of 300.13 MHz (for ^1H) and 75.47 MHz (for ^{13}C), the temperature of the probe was set at room temperature (around 293-294 K), on a Bruker Avance 400 spectrometer fitted with a 5 mm i.d. BBFO+ probe carefully tuned to the recording frequency of 400.13 MHz (for ^1H) and 100.61 MHz (for ^{13}C). The spectra are referenced to the solvent in which they were run (7.26 ppm for ^1H $CDCl_3$ and 77.16 ppm for ^{13}C $CDCl_3$, 2.50 ppm for ^1H DMSO-d_6 and 39.52 ppm for ^{13}C DMSO-d_6). Chemical shifts (δ) are given in ppm, and coupling constants (*J*) are given in Hz with the following splitting abbreviations: s = singlet, d = doublet, t = triplet, q = quartet, qt = quintet, sx = sextuplet, sp = septuplet, m = massif and br = broad. All assignments were confirmed with the aid of two-dimensional ^1H, ^1H (COSY), or ^1H, ^{13}C (HSQC, HMBC) experiments using standard pulse programs.

ESI-TOF-HRMS investigations

Intermediate and final products were characterised by electrospray (ESI)-time of flight (TOF) high resolution mass spectrometry (HRMS) measurements a Xevo G2-XS QTOF spectrometer (Waters, USA) in both positive and negative modes by direct introduction.

Synthesis of tert-Butyl (4-aminobutyl)carbamate :

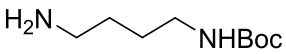

To a solution of diaminobutane (115.60 mmol, 10.36 mL) in dry DCM (100 mL) is added a solution of di-tert-butylcarbonate (57.80 mmol, 12.60 g) in dry DCM (90 mL) dropwise at 0°C. Reaction mixture is stirred at 0°C for 1h, then at room temperature overnight. The solution is diluted with DCM (200 mL). Iced-cold water is added and organic layers are extracted with DCM (3 times). Organic layers are washed with brine, dried over Na_2SO_4 and concentrated under reduced pressure. The crude is purified by flash chromatography on silica gel (DCM/MeOH, 10/0 to 8/2, 1% Et_3N) to afford compound **2** (46.24 mmol, 8.69 g) with 40% yield. ^{1}H NMR (400 MHz, $CDCl_3$): 4.80 (bs, 1H), 3.06-3.08 (m, 2H), 2.66-2.69 (m, 2H), 2.13 (bs, 2H), 1.42-1.51 (m, 4H), 1.39 (s, 9H) ; ^{13}C NMR (100 MHz, CDCl3): 156.1 (CO), 79.1 (C^{IV}), 41.6 (C_{al}), 40.4 (C_{al}), 30.49 (C_{al}), 28.5 (C_{al}), 28.5 (C_{al}), 28.5 (C_{al}), 27.5 (C_{al}) ; ESI(+)-TOF-HRMS *m/z* for $C_9H_{21}N_2O_2$ $[M + H]^+$: theoretical 189.1604, observed : 189.1603.

Synthesis of (2-(((4-((tert-Butoxycarbonyl)amino)butyl)amino)methyl)phenyl)boronic acid :

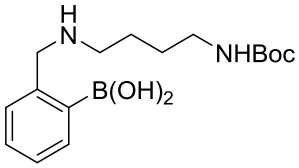

To a solution of tert-butyl(4-aminobutyl)carbamate (38.80 mmol, 7.30 g) in methanol (30 mL), is added 2-formylphenylboronic acid (38.80 mmol, 5.82 g) at room temperature, under argon atmosphere. The reaction mixture is stirred overnight at room temperature. Sodium borohydride (62.08 mmol, 2.35 g) is added carefully at 0°C. After total addition, the reaction mixture is stirred at room temperature until bubbles disappearance. Water and dichloromethane are added to the mixture. Organic layers are extracted with dichloromethane, dried over Na_2SO_4 and concentrated under reduced pressure to give compound **3** (37.05 mmol, 11.93 g) without further purification with 95% yield. ^{1}H NMR (400 MHz, MeOD): 7.43-7.45 (m, 1H), 7.13-7.21 (m, 3H), 4.00 (s, 2H), 3.10 (t, 2H), 2.85-2.89 (m, 2H), 1.71-1.79 (m, 2H), 1.50-1.57 (qt, 2H), 1.44 (s, 9H) ; ^{13}C NMR (100 MHz, MeOD): 158.5 (CO), 144.8 (C_{ar}), 142.4 (C_{ar}), 131.6 (C_{ar}), 128.2 (C_{ar}), 127.6 (C_{ar}), 124.1 (C_{ar}), 79.9 (C^{IV}), 55.0 (C_{al}), 48.6 (C_{al}), 40.8 (C_{al}), 28.8 (C_{al}), 28.8 (C_{al}), 28.8 (C_{al}), 28.6 (C_{al}), 25.2 (C_{al}) ; ESI(+)-TOF-HRMS *m/z* for $C_{18}H_{32}N_2O_4B$** $[M + H]^+$: theoretical 350.2487, observed : 350.2491.

Synthesis of (2-(((4-aminobutyl)amino)methyl)phenyl)boronic acid (wPBA):

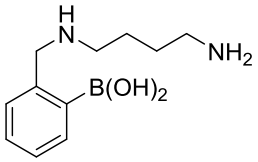

To a solution of (2-(((4-((tert-butoxycarbonyl)amino)butyl)amino)methyl)phenyl)boronic acid (2.62 mmol, 0.84 g) in methanol (5 mL), hydrochloric acid gas is bubbled (from sulfuric acid over NaCl) at 0°C under argon atmosphere. Half an hour later, methanol is evaporated. The crude is dissolved in distilled water (15 mL) and an aqueous solution of sodium hydroxide (1 M) is added until pH 11. Water is co-evaporated with toluene. The crude is dissolved in dichloromethane, dried over Na_2SO_4 and concentrated under reduced pressure to afford the wished monomer **4** (1.89 mmol, 0.42 g) with 72% yield. ^{1}H NMR (400 MHz, MeOD): 7.40-7.43 (m, 1H), 7.15-7.23 (m, 3H), 4.03 (s, 2H), 2.96-3.00 (m, 2H), 2.89-2.93 (m, 2H), 1.82-1.90 (m, 2H), 1.69-1.77 (m, 2H) ; ^{13}C NMR (100 MHz, MeOD): 144.4 (C_{ar}), 142.7 (C_{ar}), 131.5 (C_{ar}), 128.4 (C_{ar}), 127.6 (C_{ar}), 124.1 (C_{ar}), 55.2 (C_{al}), 48.2 (C_{al}), 40.4 (C_{al}), 26.7 (C_{al}), 24.7 (C_{al}) ; ESI(+)-TOF-HRMS *m/z* for $C_{11}H_{16}N_2B$* $[M + H]^+$: theoretical 186.1451, observed : 186.1443.

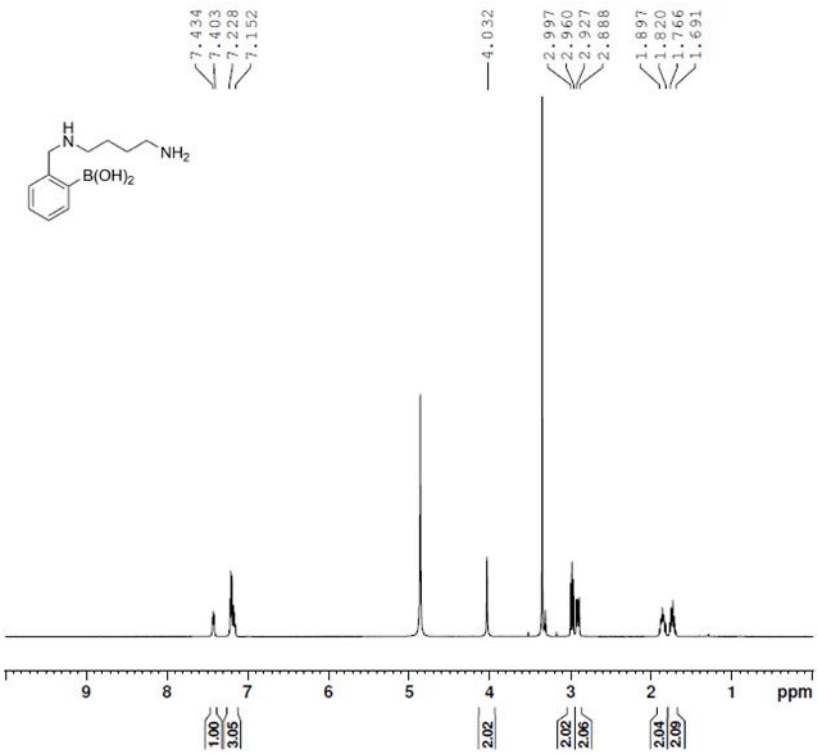

Figure S6. ^{1}H NMR spectrum of wPBA in MeOD.

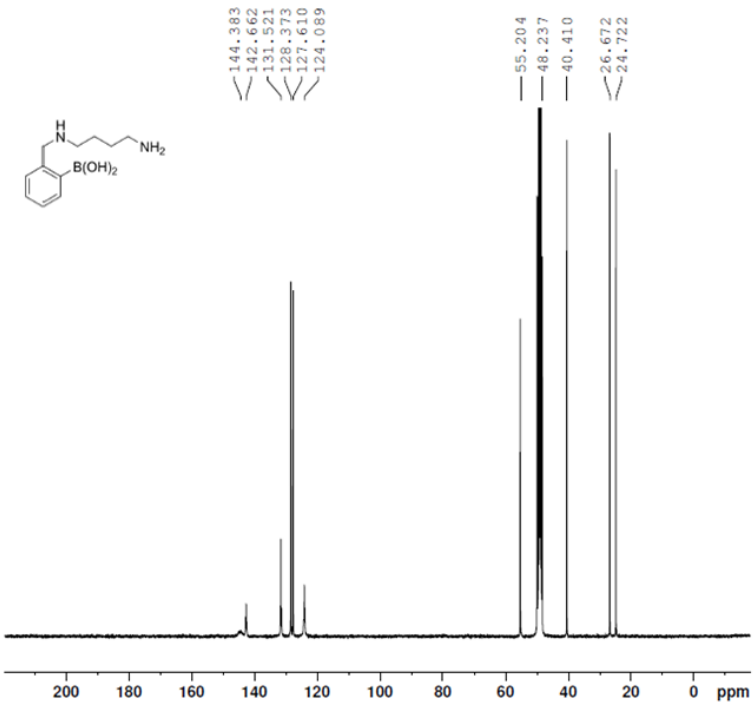

Figure S7. ^{13}C NMR spectrum of wPBA in MeOD.

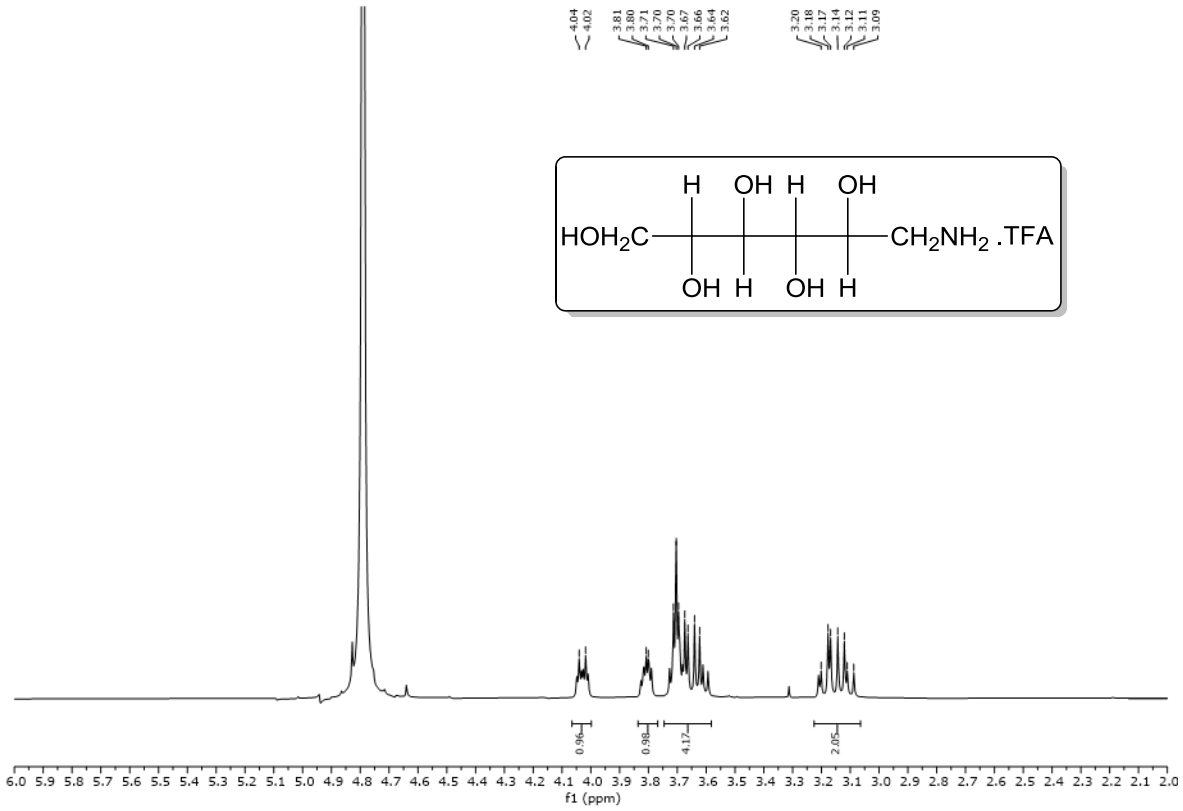

Figure S8. ^{1}H NMR spectrum of iditolamine in D_2O.

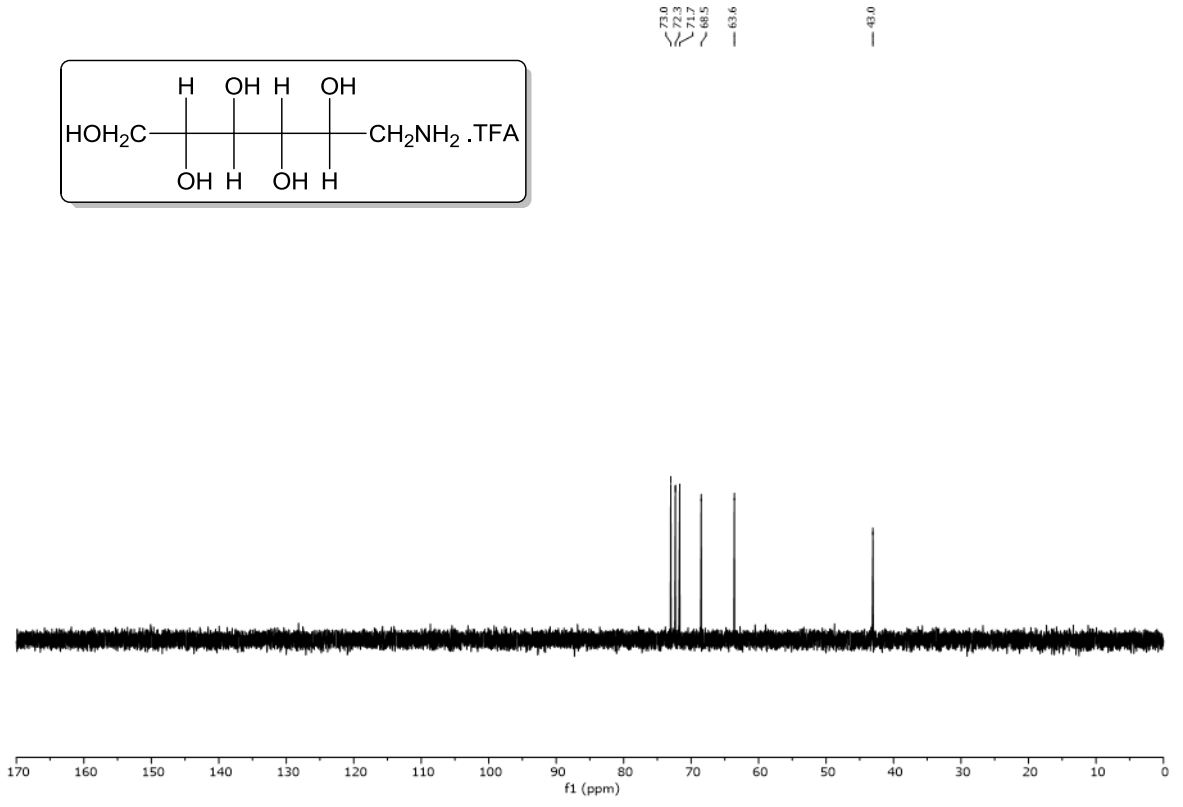

Figure S9: ^{13}C NMR spectrum of iditolamine in D_2O.

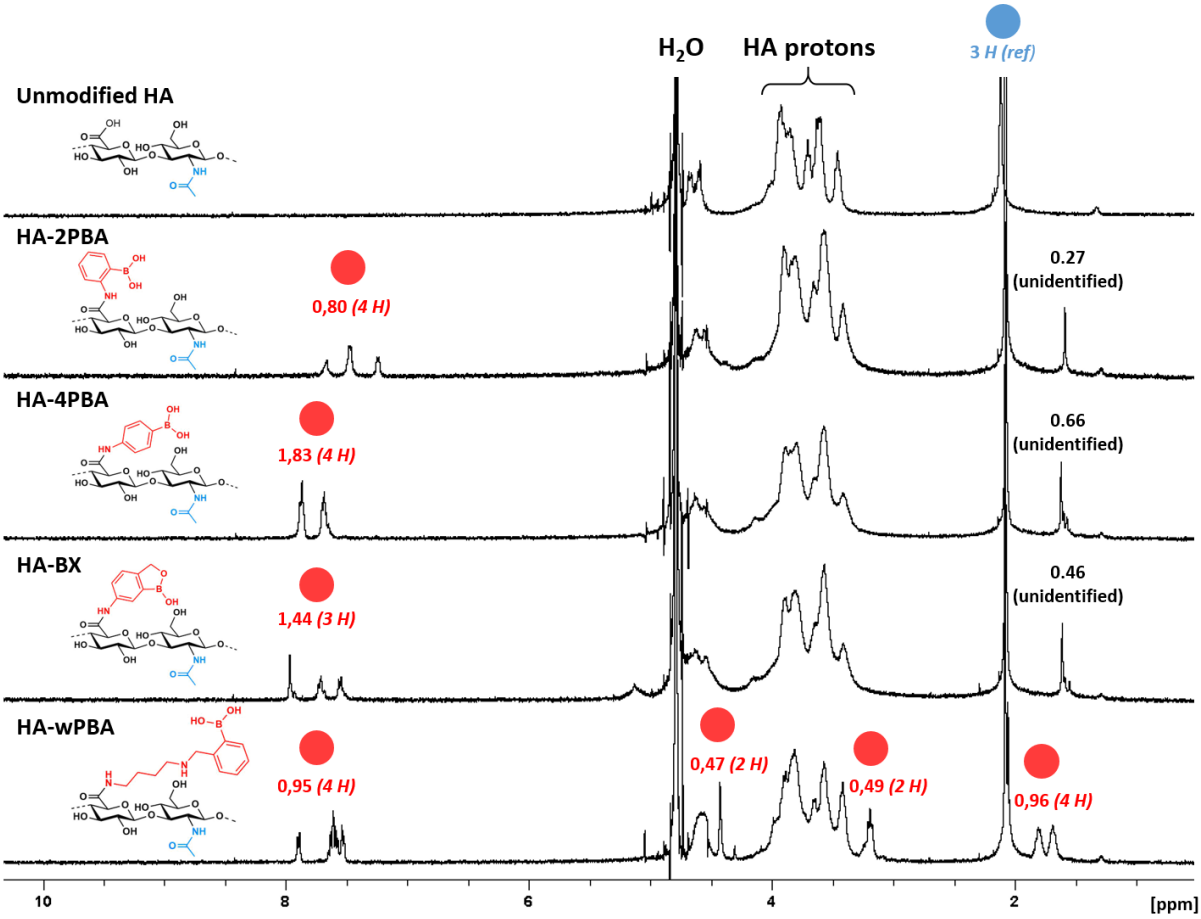

Figure S10. Representative ^{1}H NMR (400 MHz, D_2O) of HA, HA-2PBA, HA-4PBA, HA-BX and HA-wPBA, confirming the success of the syntheses. The 3 protons of the N-acetyl group of HA (blue circle, 2.1 ppm) served as a reference to calculate the degrees of substitution of HA-2PBA and HA-wPBA (red circles at 7.5-8 ppm, acounting for 3 or 4 protons). The grafting of 4PBA and BX repeatedly led to confusing substitution data via ^{1}H NMR (e.g., higher DS than the targeted values), which could not be explained. Thus, 4PBA-modified HA and BX-modified HA were characterized by another method (i.e., elemental analysis).

Table S1. Synthetic conditions for the synthesis of phenylboronic acid (PBA)-modified HA.

HA MW	Solvent	Activating agent	PBA	Substitution
300 kDa	0.1 M MES pH 5.5 (9 mL) + 1 mL DMSO	DMT-MM, 0.5 eq (34 mg; 0.124 mmol)	2PBA, 0.25 eq (11 mg; 0.062 mmol)	20% (^{1}H NMR)
			3PBA, 0.25 eq (8 mg; 0.062 mmol)	precipitate
			4PBA, 0.25 eq (11 mg; 0.062 mmol)	24% (EA)
			BX, 0.25 eq (13 mg; 0.062 mmol)	25% (EA)
100 kDa	0.1 M MES pH 5.5 (10 mL)	DMT-MM, 1 eq (69 mg; 0.248 mmol)	wPBA, 0.5 eq (28 mg; 0.124 mmol)	22% (^{1}H NMR)
300 kDa				24% (^{1}H NMR) 20% (EA)
100 kDa		DMT-MM, 2 eq (137 mg; 0.496 mmol)	wPBA, 1 eq (55 mg; 0.248 mmol)	40% (^{1}H NMR)
300 kDa				40% (^{1}H NMR)

All reactions were performed on 100 mg of HA (0.248 mmol of carboxylic acid). All equivalents were relative to the carboxylic acid groups of HA. ^{1}H NMR = proton nuclear magnetic resonance. EA = Elemental analysis.

Table S2. Synthetic conditions for the synthesis of diol-modified HA.

HA	Solvent	Activating agent	diol	Substitution
300 kDa	0.1 M MES pH 5.5 (10 mL)	DMT-MM, 1 eq (69 mg; 0.248 mmol)	Tris, 0.5 eq (15 mg; 0.124 mmol)	undetected
			Aminopropanediol, 0.5 eq (9.6 µL; 0. 124 mmol)	undetected
			Serinol, 0.5 eq (11 mg; 0.124 mmol)	undetected
			Glucosamine, 0.5 eq (27 mg; 0.124 mmol)	33% (TNBS) 29% (EA)
			Galactosamine, 0.5 eq (27 mg; 0.124 mmol)	32% (TNBS) 29% (EA)
			Fructosamine, 0.5 eq (27 mg, 0.124 mmol)	33% (TNBS) 37% (EA)
			Dulcitolamine, 0.5 eq (27 mg; 0.124 mmol)	26% (TNBS) 32% (EA)
			Iditolamine, 0.5 eq (24 mg; 0.124 mmol)	35% (TNBS)
			Dopamine, 0.5 eq (24 mg; 0.124 mmol)	undetected
100 kDa	0.1 M MES pH 5.5 (10 mL)	DMT-MM, 1 eq (69 mg; 0.248 mmol)	Glucamine, 0.5 eq (22 mg; 0.124 mmol)	33% (TNBS) 32% (EA)
300 kDa				33% (TNBS) 32% (EA)
100 kDa		DMT-MM, 2 eq (137 mg; 0.496 mmol)	Glucamine, 1 eq (45 mg, 0.248 mmol)	55% (TNBS) 52% (EA)
300 kDa				56% (TNBS) 52% (EA)

All reactions were performed on 100 mg of HA (0.248 mmol of carboxylic acid). All equivalents were relative to the carboxylic acid groups of HA. EA = Elemental analysis; TNBS = unreacted amine dosage using 2,4,6-trinitrobenzene sulfonic acid.

Table S3. Elemental analysis data of the investigated diol-modified HA, allowing to determine their degrees of substitution.

HA MW	Diol (eq)	%N	%C	N/C (m/m)	N/C (mol/mol)
300 kDa	4PBA (0.25 eq)	3.29	35.05	0.0939	0.0805
	BX (0.25 eq)	3.4	36.62	0.0929	0.0796
	wPBA (0.5 eq)	3.35	33.23	0.1008	0.0864
	glucosamine (0.5 eq)	3.456	36.176	0.0955	0.0819
	galactosamine (0.5 eq)	3.46	36.163	0.0957	0.08
	fructosamine (0.5 eq)	3.687	37.33	0.0988	0.0847
	dulcitolamine (0.5 eq)	3.62	37.36	0.0969	0.0831
100 kDa	glucamine (0.5 eq)	3.45	35.75	0.0965	0.0827
300 kDa		3.669	37.863	0.0969	0.0831
100 kDa	glucamine (1 eq)	3.97	38.38	0.1034	0.08866
300 kDa		3.72	35.92	0.1036	0.0888

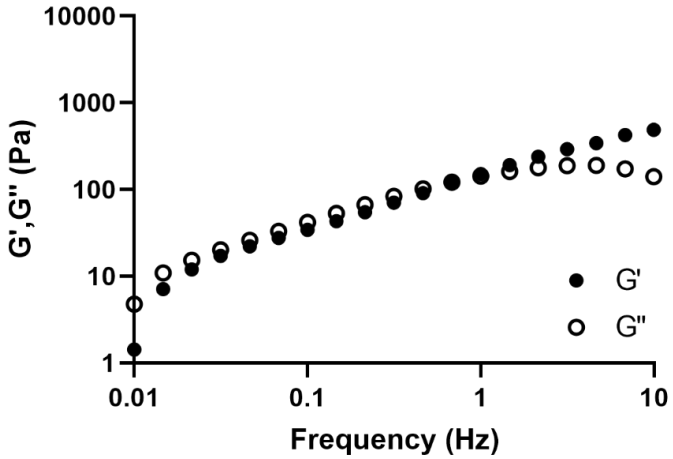

Figure S6. Frequency sweep of a wPBA/glucamine alginate hydrogels, at a total alginate concentration of 2% (w/v), using an alginate-wPBA:alginate-glucamine volume ratio of 1:1.

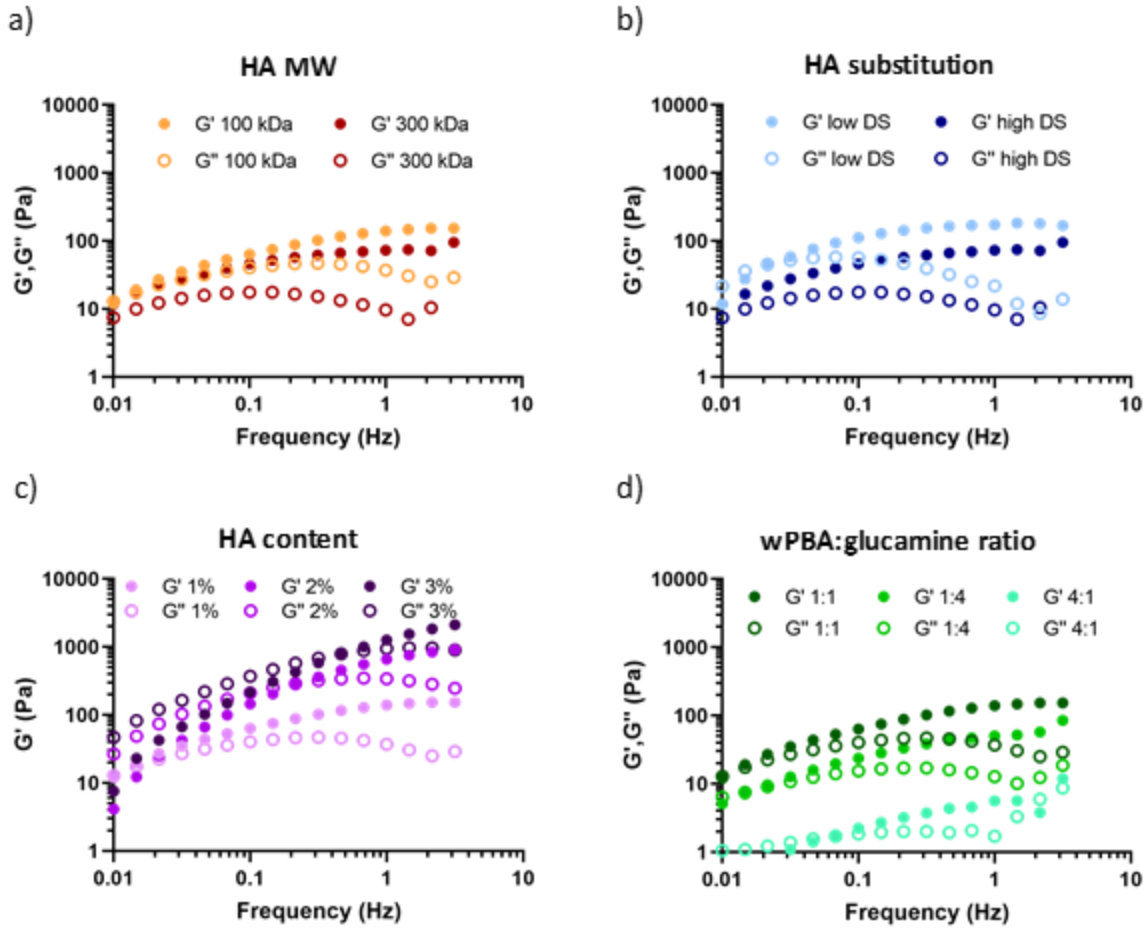

Figure S7. The influence of a) HA MW, b) HA DS, c) HA content, and d) wPBA:glucamine molar ratio on hydrogel shear elastic (*G'*) and loss (*G''*) moduli, evaluated using dynamic shear rheometry. Results on HA DS compared to low DS (HA-wPBA, 24%; HA-glucamine, 32%) and high DS (HA wPBA, 40%; HA-glucamine, 52%).

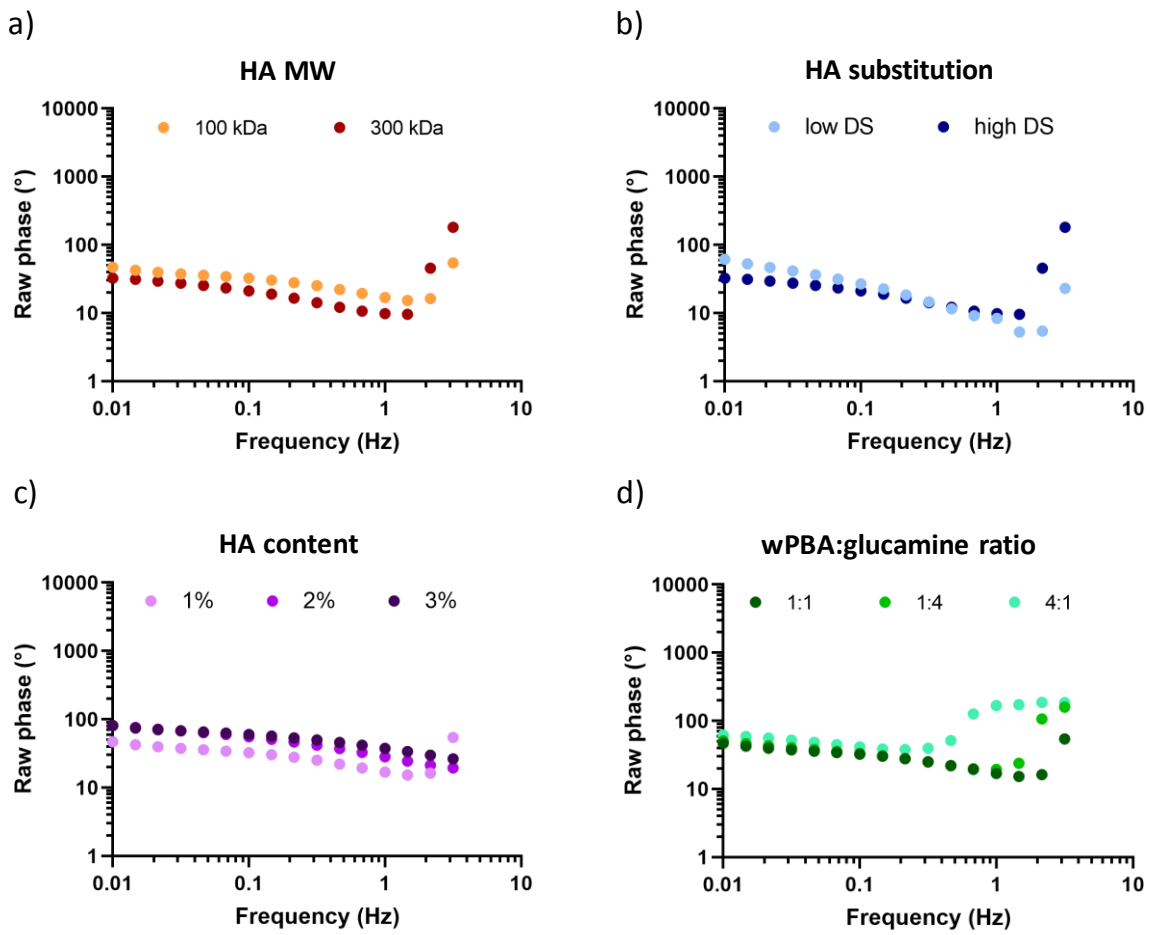

Figure S11. Raw phase data associated with Figure 2.

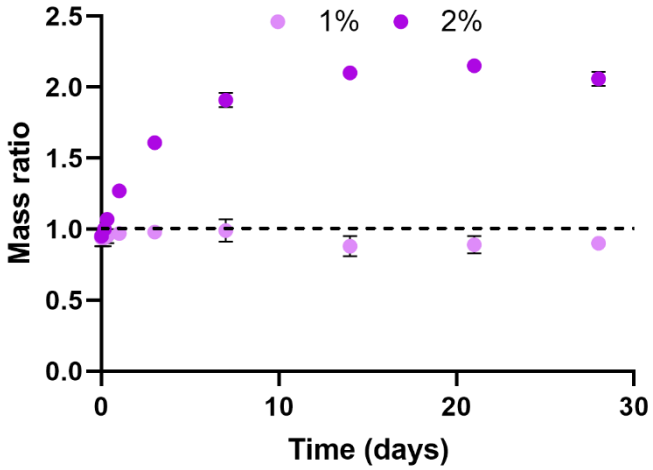

Figure S12. The influence of HA content of 300 kDa HA hydrogels (HA-wPBA: DS of 40%; HA-glucamine: DS of 52%) on the hydrogel stability/swelling. Data are shown as mean ± SD (n = 3).

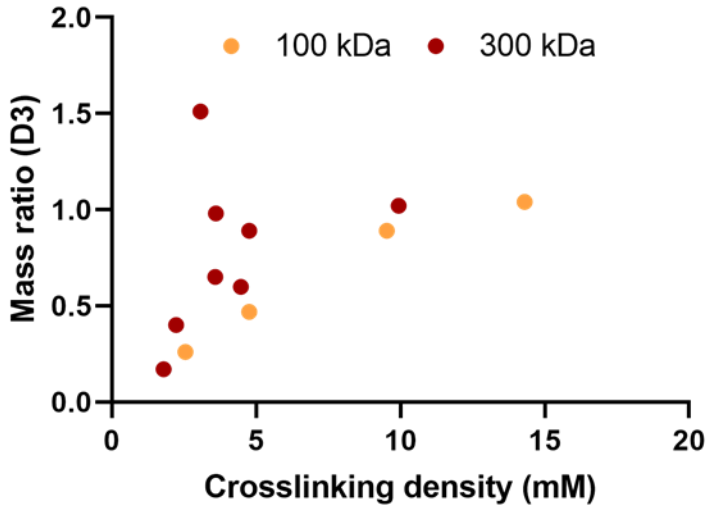

Figure S10. Swelling/shrinking behavior of immersed hydrogels as a function of the crosslinking density. Values show no obvious trend, suggesting no direct correlation. Data were extracted from the swelling/stability profiles presented in Figure 3, using the day-3 time point values.

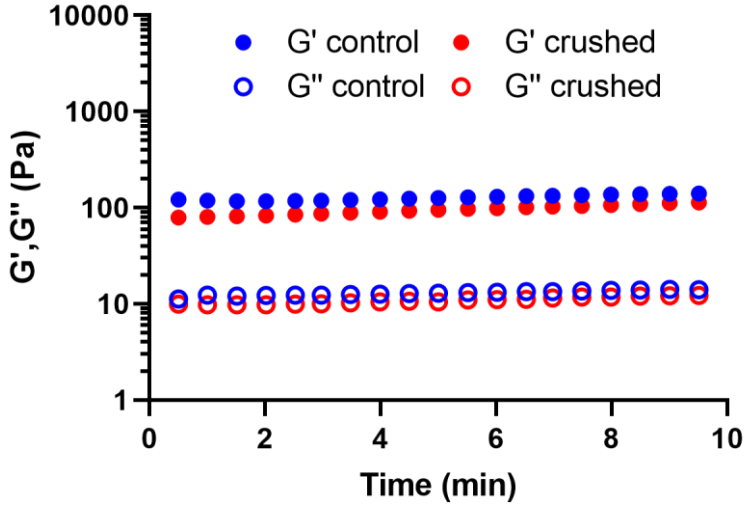

Figure S11. Rheological evaluation of a boronate ester-based hydrogel, before and after manual crushing, confirming its self-healing properties.

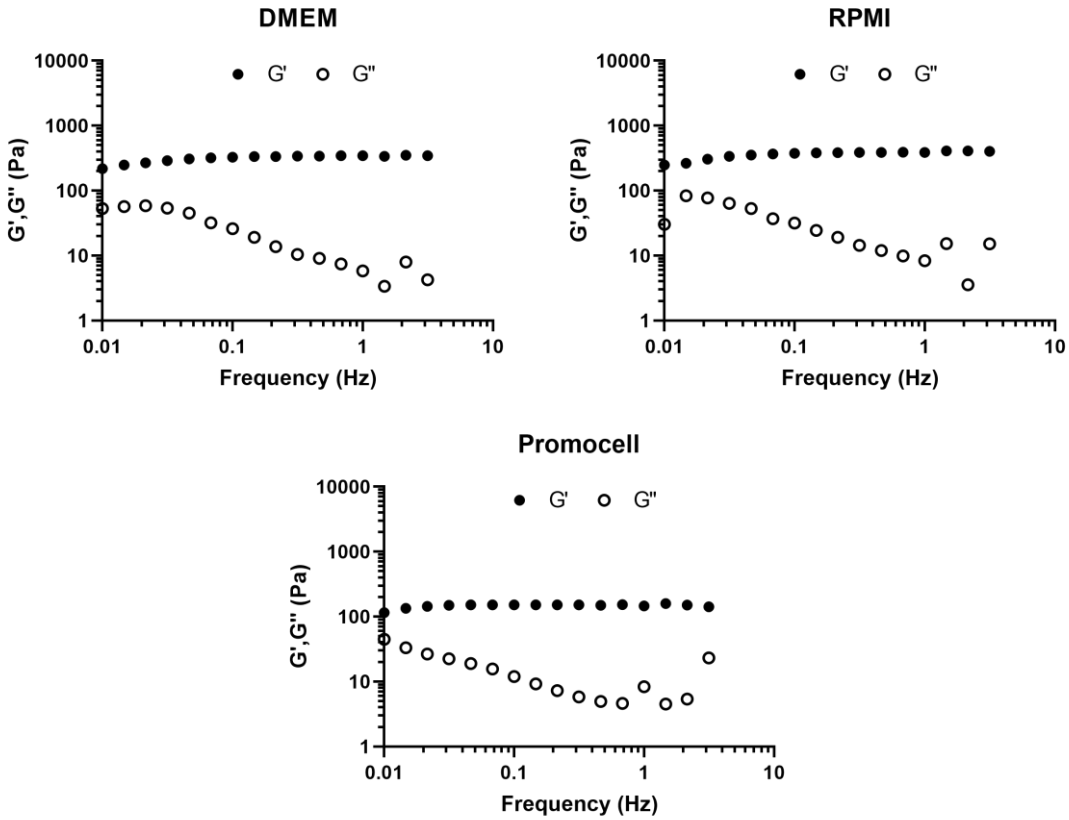

Figure S12. Our Boronate ester-based hydrogels can be obtained with a variety of cell culture media. Here, the use of DMEM, RPMI or Promocell led to successful gelation, and revealed a slight increase in the shear elastic modulus of the hydrogels in a culture medium-dependent manner.

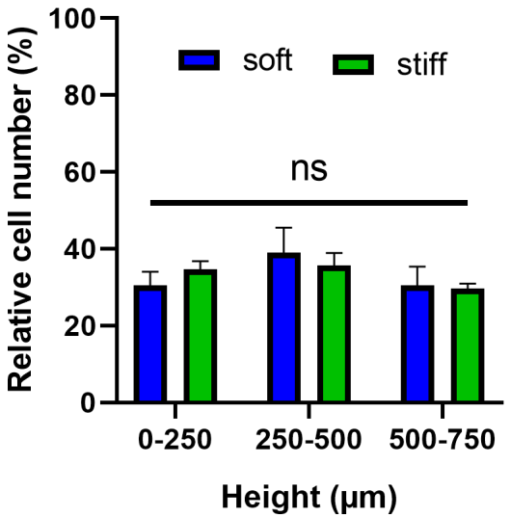

Figure S13. Relative cell distribution in the soft and stiff hydrogels, confirming homogenous cell encapsulation. The dashed line indicates the expected relative cell number in each of the three bins, which is 33%). Data are shown as mean ± SD (n = 3) with statistical significance determined using one-way ANOVA with a Tukey's post hoc test (ns : not significant).